

## Abstract

SMITH V, EDWIN RUSSELL. Estimation of Chlorophyll-a Concentrations in Nearshore Aquaculture Environments using UAV RGB Imagery. (Under the direction of Dr. Steven G. Hall and Dr. Sierra N. Young)

Freshwater-saltwater mixing dynamics, in addition to stormwater runoff, present major challenges in monitoring water quality in nearshore mariculture operations as it is difficult to maintain instruments in biologically productive brackish environments. The application of unoccupied aerial vehicles (UAVs) for water quality monitoring is expanding and can greatly reduce the burden of manually collecting water quality samples and providing accurate predictions of water quality data. An explored application of a UAV system was deployed for the estimation of surface phytoplankton concentrations via RGB imagery, water sampling, and modeling.

Experiments were conducted around a North Carolina oyster lease along the brackish North River in Straits, N.C., U.S.A. Water samples across the lease were manually collected and analyzed for their chlorophyll-a concentration, an accepted proxy for phytoplankton. Immediately before samples were collected, a UAV performed a pre-planned flight and compiled a collection of visible spectrum images over the lease. Through GIS image manipulation and statistical modeling, linear and multilinear models were created to estimate surface phytoplankton concentrations using UAV imagery. These developed methods and technologies were intended to provide nearshore aquaculture growers the ability to better predict and diagnose site productivity in a quicker, safer, and more reliable manner as compared to sampling and analysis, satellite, and multispectral UAV methods. Ongoing design and testing are expected to enhance the overall effectiveness of autonomous systems, which could have positive impacts on the environment, aquatic productivity, operation efficiency, and safety for monitoring in a variety of aquatic ecosystems.

© Copyright 2021 by Edwin Russell Smith V

All Rights Reserved

Estimation of Chlorophyll-a Concentrations in Nearshore Aquaculture Environments using UAV  
RGB Imagery

by  
Edwin Russell Smith V

A thesis submitted to the Graduate Faculty of  
North Carolina State University  
in partial fulfillment of the  
requirements for the degree of  
Master of Science

Biological and Agricultural Engineering

Raleigh, North Carolina  
2021

APPROVED BY:

---

Dr. Steven G. Hall, PhD, PE  
Committee Co-Chair

---

Dr. Sierra N. Young, PhD  
Committee Co-Chair

---

Dr. Jason K. Ward, PhD, PE

## Biography

Russell Smith was born and raised in Midway, NC. His family consisted of a bunch of avid Wolfpack fans and ever since he could remember, he wanted to be a part of the Wolfpack. Finally, he made it to NC State and decided it was the place for him. Not knowing what he wanted to do in college, he did know that he loved to go fishing. This love for fishing and math and science led him to want to become a Biological and Agricultural Engineer. After four years of undergraduate studies, he decided he wanted to stick around for two more to earn his Masters degree. He has enjoyed learning about the world of research and the topics of aquaculture and remote sensing.

# Table of Contents

LIST OF TABLES .....	v
LIST OF FIGURES.....	vi
<b>Chapter 1: Introduction</b> .....	1
1.1 Motivation .....	1
1.2 Nearshore Aquaculture Production .....	2
1.3 Phytoplankton and Chlorophyll-a .....	4
1.4 Current Methods for Phytoplankton Estimation .....	4
1.5 Hypothesis and Contributions .....	6
1.6 Organization of Thesis .....	7
<b>Chapter 2: Literature Review</b> .....	8
2.1 Sampling and Concentration Analysis .....	8
2.1.1 Sampling .....	8
2.1.2 <i>In vitro</i> Analysis .....	10
2.1.3 <i>In situ</i> Analysis .....	12
2.2 Multispectral Satellite Estimation.....	12
2.3 UAV Estimation .....	14
<b>Chapter 3: Methods</b> .....	18
3.1 Study Area.....	18
3.2 UAV Image Estimation Methods .....	20
3.2.1 UAV Data Collection .....	20
3.2.2 UAV Image Processing Workflow and Analysis .....	23
3.3 Satellite Image Estimation Methods.....	29
3.3.1 Satellite Image Collection .....	29
3.3.2 Satellite Image Analysis .....	30
3.4 Manual Grab Sampling .....	30
3.4.1 Grab Sampling Protocol .....	30
3.4.2 Sample Analysis .....	31

<b>Chapter 4: Results</b> .....	33
4.1 Summary of Data .....	33
4.1.1 Sample Analysis .....	33
4.1.2 Satellite Image Analysis .....	33
4.1.3 UAV RGB Image Analysis .....	33
4.2 Regression Analysis .....	37
<b>Chapter 5: Discussion</b> .....	48
5.1 Model Evaluation.....	48
5.1.1 Removed Data Points .....	48
5.1.2 Variability in Index Values .....	49
5.1.3 Index and Buffer Size .....	49
5.1.4 Variability in Sampled Chl-a Concentrations .....	50
5.1.5 Comparison of Estimation Method Effectiveness .....	50
5.2 Procedure Evaluation .....	50
5.2.1 Consideration of Time .....	50
5.2.2 Ease of Implementation and Model Maintenance .....	51
<b>Chapter 6: Conclusion</b> .....	52
6.1 Summary .....	52
6.2 Suggestion for Future Work .....	53
<b>References</b> .....	54
<b>Appendices</b> .....	60

## LIST OF TABLES

- Table 1. Major discoveries regarding marine phytoplankton estimation via satellite imagery
- Table 2. UAV and satellite estimation selected indices and spectral band combinations
- Table 3. Averaged Pearson correlation of chl-a with selected indices across collection points.
- Table 4. Minimum and maximum coefficient of correlation values with selected indices.
- Table 5. Description of spectral bands captured by the Landsat 8 satellite used for satellite estimation of chlorophyll-a.
- Table 6. Sample of tabular data from UAV image processing and extraction analysis
- Table 7. Sampling points and index means and standards deviations.
- Table 8. Top performing models (adjusted R<sup>2</sup>)
- Table 9. Top performing models' coefficients of correlation, standard error, and number of observations
- Table 10. Index significance in each of the top-performing models.

# LIST OF FIGURES

Figure 1. UAV water sampling; USV sampling plant biomass

Figure 2. Spectral fingerprint of chlorophyll-a displaying percent absorption according to wavelength

Figure 3. UAV and satellite chl-a concentration estimation principles

Figure 4. Study site. Intersection of Ward Creek and the North River in Beaufort, N.C., U.S.

Figure 5: Minimum, maximum, and average daily air temperature at the site over a 6-month period of this study (August 2020 – January 2021).

Figure 6: Total daily precipitation at the site over a 6-month period of this study (August 2020 - January 2021).

Figure 7: Average daily sky cover (percentage of sky obscured by clouds) at the site over a 6-month period of this study (August 2020- January 2021).

Figure 8. DJI Phantom 3 – low-cost UAV used in this study.

Figure 9: Flight plan over the study site generated in the DJI GS Pro (2.0.15) app

Figure 10. Surveyed locations for georeferencing images

Figure 11. Reference camera locations, GCPs, sampling control points, and georeferenced images in ArcGIS Pro

Figure 12. Custom raster function workflow to mask and apply indices to the UAV images.

Figure 13. Applying a mask to remove high sun reflectance and lease markers.

Figure 14. Selected indices applied to a masked image with index equations below.

Figure 15. Model within ArcGIS Pro to produce zonal statistics tables for each image based on index type and buffer size.

Figure 16. Average ExG values within the nine-foot buffer vs. true chl-a values from sampling and extraction for each

Figure 17. Average RAVI values within the nine-foot buffer vs. true chl-a values from sampling and extraction for each sampled point

Figure 18. Average nRAVI values within the nine-foot buffer vs. true chl-a values from sampling and extraction for each sampled point

Figure 19. Average ExG values within the twenty-foot buffer vs. true chl-a values from sampling and extraction for each sampled point

Figure 20. Average RAVI values within the twenty-foot buffer vs. true chl-a values from sampling and extraction for each sampled point

Figure 21. Average nRAVI values within the twenty-foot buffer vs. true chl-a values from sampling and extraction for each sampled point

Figure 22. Average ExG values within the fifty-foot buffer vs. true chl-a values from sampling and extraction for each sampled point

Figure 23. Average RAVI values within the fifty-foot buffer vs. true chl-a values from sampling and extraction for each sampled point

Figure 24. Average nRAVI values within the fifty-foot buffer vs. true chl-a values from sampling and extraction for each sampled point

Figure 25. True vs. ExG+nRAVI (20ft) model predicted chl-a concentrations ( $\text{mg}/\text{m}^3$ )

Figure 26. True vs. ExG+RAVI (20ft) model predicted chl-a concentrations ( $\text{mg}/\text{m}^3$ )

Figure 27. True vs. ExG+nRAVI+RAVI (20ft) model predicted chl-a concentrations ( $\text{mg}/\text{m}^3$ )

Figure 28. True vs. ExG+nRAVI+RAVI (9ft) model predicted chl-a concentrations ( $\text{mg}/\text{m}^3$ )

Figure 29. True vs. ExG+RAVI (9ft) model predicted chl-a concentrations ( $\text{mg}/\text{m}^3$ )

# Chapter 1 – Introduction

## 1.1 Motivation

Modern land agriculture is currently experiencing an resurgence in intelligent sensing and data analytics (Gupta, 2018; Matthews, 2019; Proagrica, 2021). It has shown to improve management practices, provide better risk assessment, transform livestock and crop care, reduce waste, increase innovation and productivity, improve profits, and improve supply chain management (Matthews, 2019; Proagrica, 2021). Precision agriculture is a big part of this transformation that relies on observation, measurement, and response to various inputs and outputs (Gupta, 2018).

Aquaculture, which is a relatively new but fast-growing sector of agriculture, can greatly benefit from the pursuit of modern optimization methods such as intelligent sensing and data analytics (Costa & Rihtar, 2016; Hall et al., 2018). To bring a new level of development to aquaculture, one must consider the state-of-the-art statistical methods and data mining techniques to gain a deeper insight into the aquaculture reality, especially through a higher frequency of sampling (Costa & Rihtar, 2016). These pursuits must also rely on the expertise of the fish farmers and the technologies they use today (Costa & Rihtar, 2016).

One subset of aquaculture that can greatly benefit from these advances in technology and methodologies is the shellfish industry. Most shellfish operations around the world are run by small family farms, usually consisting of current or former commercial fishermen looking to diversify, restaurant owners wanting to have a hands-on approach to their food supply, or individuals looking to contribute to a sustainable seafood supply or to improve the quality and productivity of their coastal waters (National Sea Grant Law Center, 2019). With rising production costs, volatile environmental conditions, and biological complexities, shellfish farmers are finding it harder to produce a profit (Chen, 2021). According to the Seafood Barometer Report (2021), there is “low added value from standalone hardware investments, but

when combined with data platforms and advanced analysis - the added value potential is huge.” This thesis intends to provide shellfish farmers with the ability to add value to their operations by focusing on the crucial input of a shellfish’s food supply by analyzing the possibility of overcoming sampling and satellite imagery technique disadvantages through experimental methods using UAV RGB imaging for chlorophyll-a concentration prediction.

## **1.2 Nearshore Aquaculture Production**

Aquaculture is the “breeding, rearing, and harvesting of fish, shellfish, algae, and other organisms in all types of water environments” (NOAA, 2019). It is a rapidly expanding industry across the United States, as well as the world, and is considered the fastest growing sector of the world food economy (White, 2018). Many researchers believe this rapid growth began following World War II when economic conditions in developed countries allowed for an increase in the demand of seafood, as well as aquaculture profitability (White et al., 2004). At this point, commercial aquaculture began to draw much attention. The continued growth and advancement of aquaculture can be attributed to many factors including advancements in logistics, food safety, nutrition, and production methods; however, there is still a large demand for innovation (Helmstetter, 2019). The industry has many significant challenges that must be overcome to meet projected demand. Many of these challenges are unique for a variety of reasons:

1. Modern commercial aquaculture has only been around for about 60 years, suggesting a lack of generational data and best practices regarding newly cultured species (Food and Agriculture Organization, 2020).
2. Coastal/open-water structures must be designed to withstand extreme hydrologic forces and not allow any escapees (The Fish Site, 2020).

3. Zoning and environmental regulations need to be developed and informed to ensure proper management and opportunities for the industry to grow (Souza, 2019).
4. Production of sustainable and nutritious feed to not deplete ocean populations further (The Fish Site, 2020).
5. Lack of environmental data acquisition to accurately monitor the health of the cultured species and mitigate environmentally posed risks

These challenges indicate that the aquaculture industry needs more data to accurately monitor and improve fish/shellfish health and production, mitigate environmental and biological risks, and better inform regulatory agencies.

This thesis is focused on the shellfish industry and how UAV imagery can provide valuable information regarding the health of the shellfish and surrounding ecosystem. In 2016, shellfish aquaculture accounted for approximately 21.4% of world aquaculture production in terms of live weight (FAO, 2018). This is roughly equivalent to 17 million tons of shellfish. The United States contributed around 23 thousand tons, while North Carolina contributed 327 tons (NOAA, 2020; Wagner, 2018). North Carolina's production numbers may seem relatively low, but the shellfish industry is nonetheless important to the state and several of its coastal communities.

Opportunities to start a shellfish business in N.C. are also expanding as the number of water column and bottom leases increase (N.C. Division of Marine Fisheries, 2020). Leases are managed by the governing state. On these leases, the shellfish "seed" that are purchased from either a hatchery or nursery are placed on structures on the seafloor or in floating mesh bags or cages near the surface for the grow-out phase (Nell, 2002). Throughout the next 12-18 months, the oysters are cleaned and graded based on size and shape until they are ready to be harvested and processed for market (Kallen et al., 2001).

### **1.3 Phytoplankton and Shellfish Health**

Shellfish, including oysters, mussels, scallops, and clams, are filter feeders, meaning they obtain their food by straining suspended matter and food particles from the surrounding water (Duncan, 2003). Naturally, their diets primarily consist of phytoplankton (Weissberger & Glibert, 2021). Phytoplankton are photosynthetic, microscopic algae that can either be unicellular, colonial, or filamentous. They are a significant food source for zooplankton and aquatic filter-feeding organisms, such as shellfish (Rice et al., 2018). It is also estimated that phytoplankton contribute between 50 to 80 percent of the oxygen in Earth's atmosphere; 20 percent coming from one species in particular, *Prochlorococcus* (NOAA, 2021). When in coastal/transitional environments with low phytoplankton concentrations ( $<1.0 \text{ mg/m}^3$ ), the shellfish will die or have stunted growth (European Environment Agency, 2021). Extremely high phytoplankton concentrations in these waters ( $>20 \text{ mg/m}^3$ ) can promote the formation of harmful algal blooms (HABs) which can cause extreme complications for marine life (Powell et al., 1995). For these reasons, it is concluded that effects on marine phytoplankton concentrations should be included in management deliberations (Tweddle et al., 2018). Being able to quickly, safely, and accurately monitor concentrations of phytoplankton can enable shellfish growers to monitor the health of their crop and potentially mitigate environmental risks.

### **1.4 Current Methods for Phytoplankton Estimation**

There are several methods used to estimate phytoplankton concentrations. The true concentration of phytoplankton in a given volume of water is determined by laboratory analysis. One method involves manually counting cells either with a microscope or a flow cytometer (Karlson et al., 2010). In other methods, concentrations of phytoplankton are often analyzed by proxy of Chlorophyll-a (chl-a), a pigment present in phytoplankton (Blondeau-Patissier et. al. 2014). Chl-a has a unique absorption spectrum allowing special instruments to accurately detect

the pigment and its concentrations. These methods include in-vitro fluorometry, spectrophotometry, and liquid chromatography (Faust & Norris, 1985; Blondeau-Patissier et al. 2014). These processes are typically effective but can be tedious and time-consuming. Some submersible fluorescence sensors have been developed for in-situ measurement, but these still require the user to travel to the lease site, which may be unnecessary (Gregor et al., 2005). More modern methods used to estimate marine phytoplankton concentrations involve remote monitoring.

Remote monitoring, the alternative to sampling utilizing a network of sensors and datalogging devices, can enhance the understanding of the environment around us and how humans affect various ecosystems (Nam et al., 2015; Pinto et al. 2013). Remote monitoring of marine environments can be accomplished by fixed systems, such as buoys or fixed weather monitoring systems, or by continually moving systems, such as satellites. Fixed sensor networks have been popularized by their ability to remotely collect large amounts of data simultaneously; however, they are often limited by their inability to move (Pinto et al. 2013). Satellites are also commonly used to monitor our oceans. Satellites allow for marine systems to be analyzed on a very large scale, while being easily accessible to most users (Von Tress et al., 2021). Depending on the resolution of the satellite images, smaller, more localized systems may require other forms of sensors to achieve the level of precision necessary for a detailed analysis of the study area. Earth observation satellites, such as the Landsat 8 satellite, have been utilized to estimate surface marine phytoplankton (Candido et al., 2016). The Landsat 8 satellite produces multispectral images every 16 days with a 30-meter spatial resolution. It includes eleven spectral bands, four of which are used in the estimation of Chlorophyll-a. The process of satellite estimation begins by retrieving a multispectral image, splitting the image into its various spectral bands and generating band combinations to produce the indices necessary to detect Chlorophyll-a. The time taken between imaging and the image's spatial resolution limits its usefulness for the analysis of a small area or shellfish operation.

In many applications, automated vehicle systems, whether aerial or surface, can enhance data acquisition and decision making (Smith et al. 2015). These technologies allow researchers to collect large amounts of data while essentially eliminating the need to manually collect samples, which is often time-consuming and occasionally dangerous. The introduction of uncrewed vehicles for remote monitoring has expanded researchers' abilities to collect data in ways that have previously been challenging or impossible. This is especially true in coastal water quality monitoring.

## **1.5 Hypothesis and Contributions**

It is hypothesized that UAV imagery can provide an accurate estimation of phytoplankton concentration in nearshore aquacultural environments. Estimation via UAV is intended to mitigate risks associated with water sampling, make the process quicker and more widely available to shellfish growers. The objectives of this thesis are to: (1) increase the resolution of remote image estimation, (2) compare the efficacy of common thematic band combinations (indices), (3) create a robust model that is applicable to various coastal environments, and (4) achieve UAV RGB image estimation accuracy comparable to satellite estimation methods.

This work is intended to lay the foundation for an autonomous UAV/USV system for sampling and surface marine phytoplankton concentration estimation and modeling. There are numerous fields in which collaborative heterogeneous systems are already being developed. Acute challenges such as response to natural disasters or emergency situations are one area of application, but other times more chronic or intermittent impacts must be sensed and managed. Environmental agencies and aquatic industries have started to capitalize on these systems. Collecting accurate environmental data can help people make more informed decisions on whether to manipulate a target environment and if so, to the extent which is necessary. The

overarching goal of these systems is to mitigate environmental and safety risks through precise data collection and/or environmental manipulation.

## **1.6 Organization of Thesis**

This thesis is organized as follows:

- Chapter 2 begins with a literature review on marine phytoplankton concentration estimation methods including manual sampling and satellite estimation, as well as the inclusion of uncrewed autonomous vehicles in the process.
- Chapter 3 contains a detailed description of the study site including a brief narrative on the oyster operation, as well as weather patterns across the study period. It also includes the methodologies of UAV data collection and estimation, satellite estimation, and sampling of surface marine phytoplankton.
- Chapter 4 presents the results from sampling, UAV estimation, and satellite estimation including chlorophyll-a values from sampling, indexed aerial and satellite images and values, predicted chlorophyll-a concentrations, and estimation models for each of the three indices.
- Chapter 5 includes discussion on the practicality and accuracy of a UAV model for marine phytoplankton concentrations as compared to satellite estimation and sampling.
- Chapter 6 summarizes the conclusions of the objectives presented within this thesis, as well as special considerations and recommendations for future research.

## Chapter 2 - Literature Review

### 2.1 Sampling and Concentration Analysis

Sampling and analysis of a marine waters provides an enhanced understanding of the chemical and biological complexities contained there within. This section outlines the various ways sampling of marine phytoplankton and concentration analysis can be accomplished.

#### 2.1.1 Sampling

There are many factors to consider when manually collecting marine surface samples for biological evaluation including safety, sampling scheme, preservation of sample integrity, chain of custody, and documentation (Decker & Simmons 2013). Anytime manual sampling is required, proper precautions according to site and method-specific health and safety plans must be observed. For marine surface sampling, weather and hydrologic conditions become extremely pertinent to the safety of the sampling crew. Before sampling can occur, a sampling scheme must be developed. This includes the type of data, number of samples and equipment needed, sampling technique, and the location of each proposed sample. For example, surface phytoplankton samples are typically collected shallower than the chlorophyll maximum depth, which is around two to eight meters below the water's surface (Kolb et. al. 2016). The Florida Department of Environmental Protection outlines several surface water sampling techniques including the direct grab technique, sampling with an intermediate vessel or container, pump and tubing, and sampling in shallow water (FDEP 2017). The direct grab technique involves removing the container cap and slowly submerging the container, opening first, into the water. The bottle is then inverted so the opening is upright and is pointing in the direction of oncoming water flow, slowly allowing the water to fill the container. Sampling should be done where unwanted sampling material or other possible contaminants of concern can be avoided if

possible. When grab sampling, the location of each sample should be recorded. Once samples are retrieved, the proper preservation and handling techniques for the particular application should be adhered to. For phytoplankton preservation, samples need to be kept in opaque containers and away from sunlight and can only be handled in subdued lighting as the chlorophyll pigment is sensitive to light and can degrade. Chlorophyll is also sensitive to heat so samples should be transported on ice and stored in the refrigerator for up to two hours until filtration (FDEP 2010, EPA 2013). Samples also need to be properly labeled with a chain of custody and possible deviations from the procedure being documented. Given these procedural considerations, manual sampling can often be time consuming and can be prone to introducing errors.

Another way to sample marine surface water is with autonomous sampling devices or uncrewed remote vehicle systems. Autonomous sampling can replace manual sampling and can provide continuous or high frequency monitoring. It can also allow monitoring to be accomplished in remote or otherwise inaccessible areas. Autonomous sampling devices generally consist of sensors and pumps to periodically fill sampling vessels based on various parameters, such as time, flow, or water quality conditions. Autonomous vehicle systems, such as uncrewed surface vehicles (USV) and uncrewed aerial vehicles (UAV), are being used in a variety of ways to collect marine surface samples (Ore et al., 2015; Taylor et al., 2014).

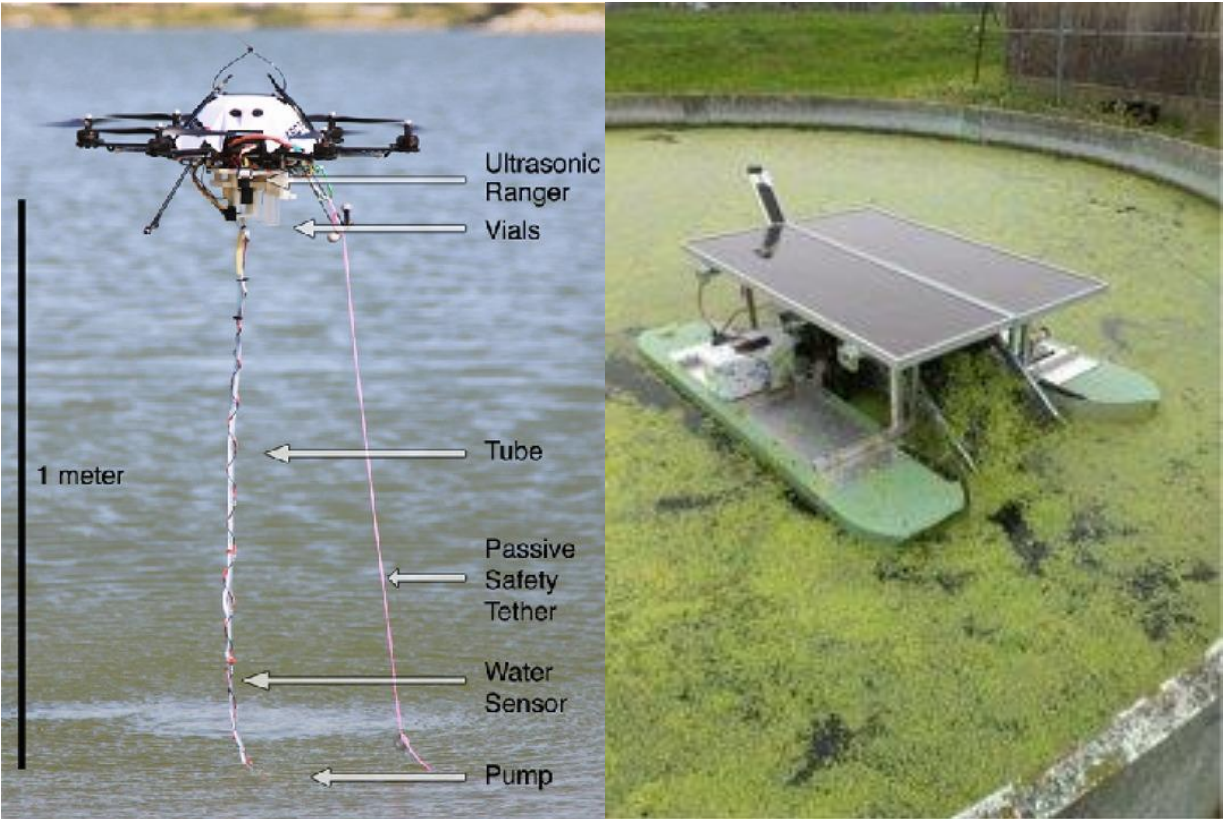


**Figure 1. UAV water sampling (left; Ore et al., 2015); USV sampling plant biomass (right; Taylor et al., 2014)**

USVs can be equipped with sensors, pumps, and sample containers and can be programmed to travel and collect samples based on predetermined locations or water quality conditions. UAVs are being used in similar ways. The advantages of using these vehicles include vastly increasing the speed and range of collection while reducing cost and effort (Ore et al. 2015). After collection, the samples can be analyzed using *in vitro* methods.

2.1.2 *In vitro* Analysis

The concentration of marine phytoplankton can be determined by a variety of *in vitro* methods including manual cell counting, spectrophotometry, high performance liquid chromatography (HPLC), and fluorometry (Faust & Norris, 1985; Blondeau-Patissier et. al. 2014). When sampling for surface marine waters, spectrophotometry is a common method used

for analysis. Like other *in vitro* methods, spectrophotometric estimation of phytoplankton relies on the detection of chlorophyll-a, a predominant pigment found in green plants and algae that is essential for oxygenic photosynthesis (Cullen 1982, EPA 2016). This type of chlorophyll absorbs light in the violet to orange spectrum at 400-700 nm and reflects light in the green spectrum at 500-570 nm (NCBI 2021). This method, as described by the Florida Department of Environmental Protection (2010), involves the filtration of a water sample through a glass fiber filter to remove any debris and to concentrate chlorophyll-containing organisms. Mechanical rupturing of the cells is then performed to allow the extraction of chlorophyll into the organic solvent acetone. The extract's absorbency is then analyzed by a spectrophotometer at specific wavelengths to detect chlorophyll-a concentration based on the pigment's unique spectral fingerprint, shown in Figure 2 (FDEP 2010).

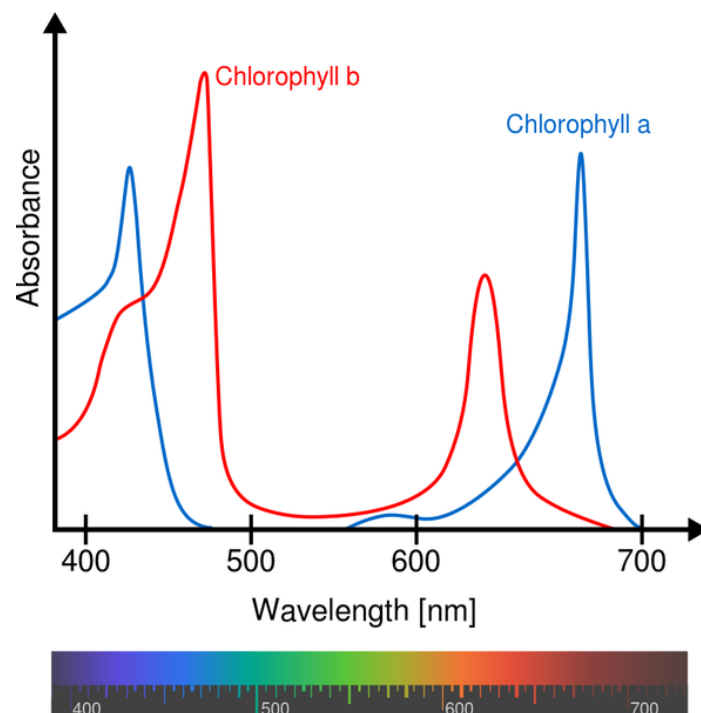


**Figure 2. Spectral fingerprint of chlorophyll-a displaying percent absorption according to wavelength (Milne et al., 2015)**

The concentration of chlorophyll-a can then be used to estimate phytoplankton concentrations.

### 2.1.3 *In situ* Analysis

*In situ* solutions have also been developed to determine chlorophyll-a concentrations in marine environments. Chlorophyll fluorescence measurement is a sensitive and effective quantification method due to improvements in optical design, electronic technology and calibration protocol and works without disrupting the cells (Zeng & Li, 2015). Many commercial *in situ* chlorophyll fluorometers are available and generally consist of a light source, detector, light guide, wavelength-selection device, and signal processing electronics (Zeng & Li, 2015). This solution has been developed to be used in spot sampling and continuous monitoring applications; however, it is often recommended to combine *in situ* sampling with extractive analysis to ensure high accuracy (Kuha et al., 2019).

## 2.2 Multispectral Satellite Estimation

Major developments in remote sensing and marine science technologies have led to the large-scale estimation of phytoplankton concentrations in marine environments (Babin et al., 2008; Blondeau-Patissier, 2014). Remote sensing using observation satellites drastically reduces the time, equipment needed, and risks associated with manual sampling as it relates to the estimation of marine phytoplankton concentrations. These technologies and methodologies also provide a greater synoptic view of marine environments, both temporally and spatially (Blondeau-Patissier, 2014). As with extractive phytoplankton estimation methods, satellite estimation relies on the proxy of chlorophyll-a. Many major discoveries from this technology have been made (Table 1).

**Table 1. Major discoveries regarding marine phytoplankton estimation via satellite imagery**

<b>Study Summary</b>	<b>Source</b>
Higher concentrations of chl-a are located along the coasts and continental shelves, north of 45° N (greater nutrient supply)	Cullen, 1982
Moderate concentrations of chl-a are located along the Atlantic and Pacific equatorial waters (upwelling between ocean masses)	Cullen, 1982
Moderate concentrations of chl-a also found in the subtropical convergence zone, south of 45° S (cool, nutrient-rich sub-Antarctic waters mix with warm, nutrient-poor subtropical waters)	Cullen, 1982
Deep chlorophyll maxima (DCM) inconsistently captured by satellites	Cullen, 1982 Huisman et al., 2006
Extremely low or deep chl-a concentrations are unreliably found by satellites, but are known to occur	Dore et al., 2008 Villareal et al., 2011
Large area estimations are difficult to model due to high variability distributions	Martin, 2003
Satellite imagery estimation of chl-a is the primary technique in areas of bloom regularity in specific regions or unexpected area (oligotrophic gyres)	Wilson, 2003 Wilson et al., 2008 Wilson, C. & Qiu, X., 2008
Second and third generation satellite ocean color sensors greatly improved chl-a estimation accuracy	Shen et al., 2012

These discoveries provide researchers with an idea as to what concentrations can be found in what areas, areas of unreliability, and which ocean color sensors provide the greatest accuracy.

Although satellite imagery has been proven to provide accurate phytoplankton estimation

models on a large-scale, it does have a few drawbacks that limit its usefulness for particular applications. With set imaging schedules, sometimes weeks apart, rapid changes in an environment may not be captured. Low image resolution may also provide a limitation to the amount of information that can be gathered within a certain area to accurately assess the environment. One of the biggest issues in satellite imagery techniques is the corruption of an image due to atmospheric conditions i.e., clouds (Al-Wassai & Kalyankar, 2013). These drawbacks are why some researchers have focused their attention on the use of UAVs.

### **2.3 UAV Estimation**

UAVs, whether fixed-wing or multicopter platforms, are becoming an increasingly popular solution for environmental monitoring as they can provide access to physically inaccessible environments, collect high resolution data, and can be equipped with various sensor payloads. Depending on the application, there are both expensive high-end specialist solutions as well as low-cost, off-the-shelf commercial options (Green et al., 2019). For the application of phytoplankton concentration estimation, the proposed benefits of using low-cost UAVs include automated rapid deployment and collection, increased user safety, high resolution imagery and modelling, and increased access to current environmental conditions. Figure 3, below, demonstrates the principles associated with UAV image estimation of phytoplankton concentrations.

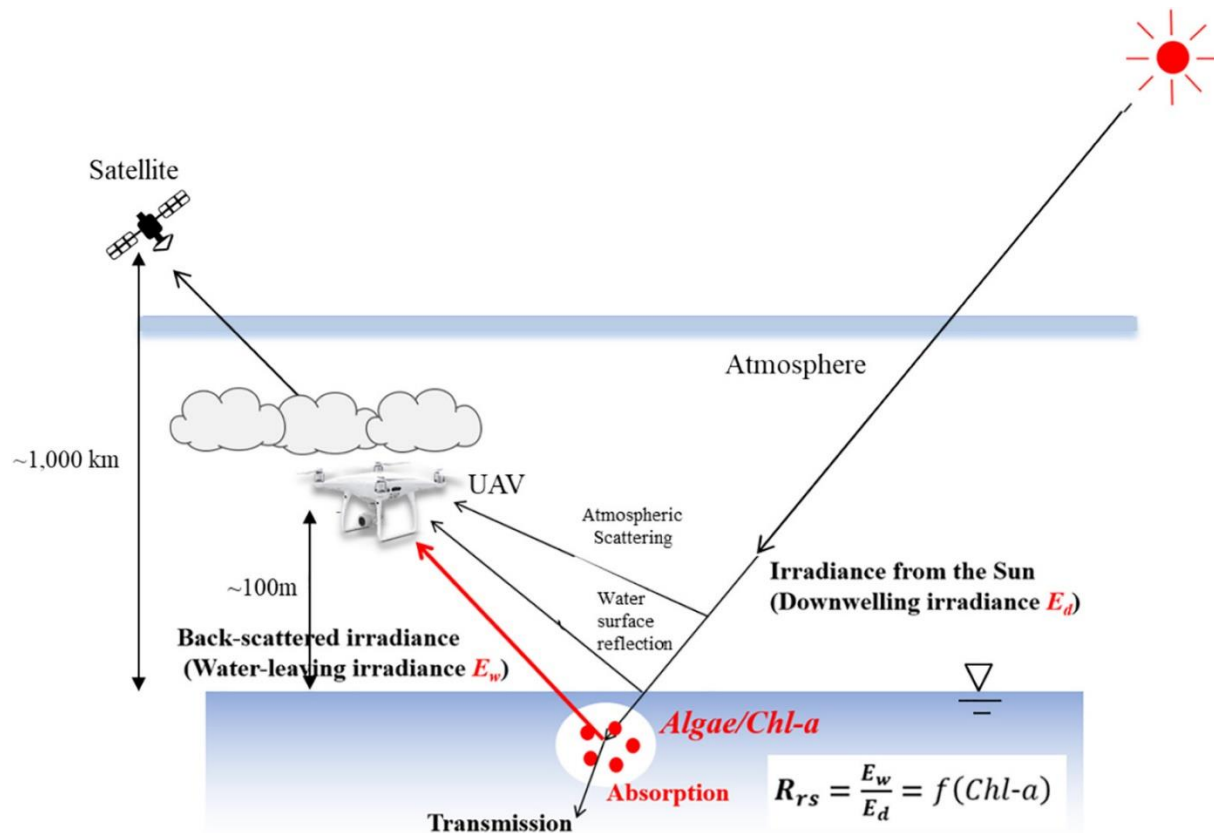


**Figure 3. UAV and satellite chl-a concentration estimation principles**

Figure 3 also demonstrates one of the drawbacks to satellite image estimation, weather. With images being taken of an area on a set time interval, this issue can drastically delay the retrieval of valuable data. UAV imagery can also provide higher resolution images as compared to satellite imagery allowing for a more detailed analysis, especially when working with small-scale oyster leases.

Currently, many UAV solutions rely on multispectral imagery like that of satellites. These models rely on the addition of the near-infrared (NIR) band to the typical image bands of red, green, and blue (RGB). Many low-cost UAVs are not equipped with a specialized NIR camera, which is a reason why this thesis explores the possibility of estimating marine chl-a concentrations without the need of a NIR band in the modeling process. UAV RGB imagery methods have been explored for chl-a estimation but only in freshwater environments (Candido

et al., 2016). In this study, three indices were compared using both satellite (Landsat 8) and aerial imagery. Those indices were: Excess Green (ExG), Ratio Aquatic Vegetation Index (RAVI), and normalized Ratio Aquatic Vegetation Index (nRAVI). The Normalized Difference Vegetation Index (NDVI) was also analyzed for satellite imagery, as it relies on the NIR band. These indices band combinations are shown in Table 2.

**Table 2. UAV and satellite estimation selected indices and spectral band combinations**

<b>Index</b>	<b>Band Combination</b>
RAVI	Green / Red
nRAVI	$(\text{Green} - \text{Red}) / (\text{Green} + \text{Red})$
ExG	$2 * (\text{Green}) - (\text{Red} + \text{Blue})$
NDVI	$(\text{NIR} - \text{Red}) / (\text{NIR} + \text{Red})$

The average Pearson correlation values from this study according to index and imagery method are shown in Table 2 and minimum and maximum coefficient of correlation values are shown in Table 3.

**Table 3. Averaged Pearson correlation of chl-a with selected indices across collection points.**

Images	Correlation				
	Point	Chl-a/RAVI	Chl-a/nRAVI	Chl-a/ExG	Chl-a/NDVI
Aerial photos	1	-0.9228125	-0.9798255	-0.8660254	-
	2	-0.9977289	-0.9901745	-0.9878292	-
	3	-0.933207	-0.9624829	-0.9707253	-
	4	-0.958918	-0.9973936	-0.9707253	-
Landsat 8 images	1	-0.9987576	-0.999806	-0.9707253	0.9788183
	2	-0.9273513	-0.9998575	-0.9912407	0.9932493

**Table 4. Minimum and maximum coefficient of correlation values with selected indices.**

Images	Indices	Minimum R <sup>2</sup>	Maximum R <sup>2</sup>
Aerial photos	RAVI	0.8516	0.9955
	nRAVI	0.9264	0.9948
	ExG	0.7500	0.9758
Landsat 8 images	RAVI	0.8600	0.9975
	nRAVI	0.9996	0.9997
	ExG	0.9243	0.9826
	NDVI	0.9581	0.9865

Candido et al. (2016) concluded that there was a “high correlation between vegetation indices generated from aerial photographs and Landsat 8 images with chlorophyll-a water extracted in the laboratory.” This suggests that UAV RGB imagery methods provide a feasible solution for phytoplankton estimation in freshwater reservoirs; however, attempts in marine environments have yet been conducted before the study described in this document.

## Chapter 3 – Methods

A correlational study was conducted to assess and compare the accuracy of satellite, UAV, and grab-sampling estimation of phytoplankton concentrations in reference to spectrophotometrically verified concentrations. This section contains descriptions of the study area, methods of sample and image collection, and sample and image processing.

### 3.1 Study Area

This study took place over a two-acre, cage-culture oyster lease in Beaufort, North Carolina, U.S., at the intersection of Ward Creek and the tidal North River (Figure 4).



**Figure 4. Study site. Intersection of Ward Creek and the North River in Beaufort, N.C., U.S. (Image courtesy of Google Maps).**

This oyster lease is typical for what is found in North Carolina regarding size and grow-out methods (N.C. Division of Marine Fisheries, 2021). Based on observation, the lease depth typically ranges from three to four feet. The seafloor underneath the lease is subtidal, hard, and has little vegetation or shells (NCSitingTool, 2021). Since accessibility to the lease is also a factor in site selection, the study location chosen was near both a dock and boating ramp. The National Weather Service provides historical climate data from the Beaufort Smith Field (KMRH)

airport weather station; less than five miles away (National Weather Service, 2021). Average annual air temperature, precipitation, and sky cover are shown in Figures 5-7.

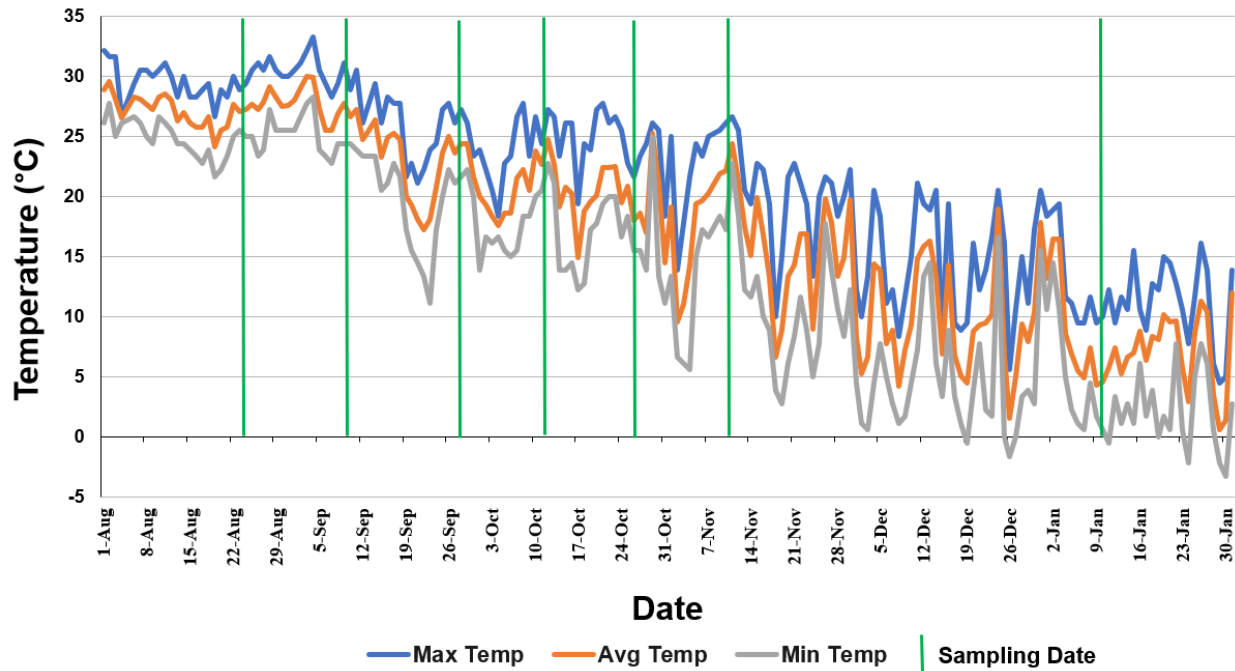


**Figure 5: Minimum, maximum, and average daily air temperature at the site over a 6-month period of this study (August 2020 – January 2021).**

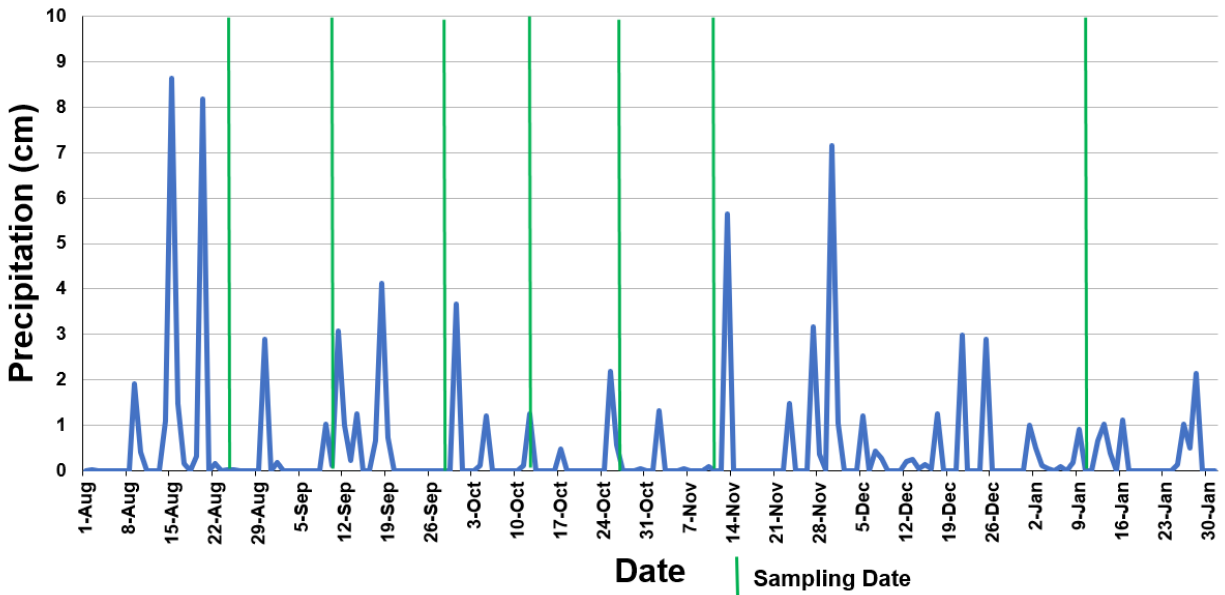


**Figure 6: Total daily precipitation at the site over a 6-month period of this study (August 2020 - January 2021).**

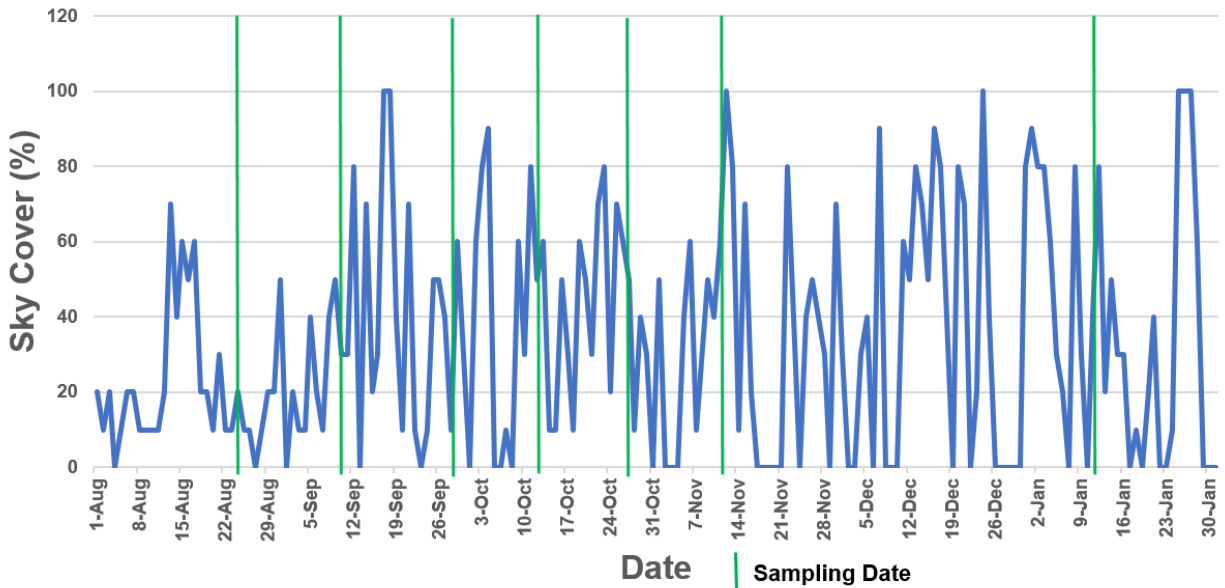


**Figure 7: Average daily sky cover (percentage of sky obscured by clouds) at the site over a 6-month period of this study (August 2020- January 2021).**

## 3.2 UAV Image Estimation Methods

### 3.2.1 UAV Image Collection

Each day of the study began with UAV imaging of the site. A DJI Phantom 3 Standard (SZ DJI Technology Co., Shenzhen, Guangdong, China), pictured in Figure 8, was used to collect the RGB images. This multirotor UAV is controlled by an app available in iOS or Android. It also has a GPS and IMU (inertial measurement unit) to keep detailed records of flight data. It is equipped with a 12-megapixel RGB camera and gimbal to control the camera’s vertical angling. The UAV can be piloted manually or autonomously and can fly up to twenty-five minutes on a single charge. It is also lightweight and portable (DJI, 2015).



**Figure 8. DJI Phantom 3 – low-cost UAV used in this study.**

Flight planning and operation was conducted through the DJI GS Pro app (version 2.0.15, Shenzhen, China). One of these flight plans is shown in Figure 9.



**Figure 9: Flight plan over the study site generated in the DJI GS Pro (2.0.15) app**

This flight plan was designed to autonomously capture the entire oyster lease, as well as all ground control points (GCPs). GCPs are points on the ground with known locations. Each flight was at 100 m (328 ft) AGL (above ground level). This flight height is below the allowable

400 ft set forth by the FAA Small Unmanned Aircraft Systems Part 107 (Small Unmanned Aircraft Systems, 2021). Each image taken at this height can cover approximately 0.07 hectares (0.17 acres), with a ground sampling distance (GSD) of 0.045 m. The GSD is the distance from one pixel to the next in reference to the ground. Horizontal and vertical image overlap was set to 80%, meaning each image consists of 80% of the information of the previous image and 20% of new information. A high image overlap provided multiple pictures of each sampling point per flight.

Before each flight, ground control points were established and initialized. These white marks, shown in Figure 10, serve as a spatial reference for when the UAV images are georeferenced in the GIS correction process. A short static survey was conducted using three GPS receivers two of which were near the shore (~6 m) and the other away from the shore (~23 m). This practice is consistent with general short, static surveying techniques. The survey was completed using Spectra SP80 GNSS receivers and Survey Pro (6.6.3, Trimble Inc., Sunnyvale, CA).



**Figure 10. Surveyed locations for georeferencing images**

All flights began with a visual inspection of the flight area for any obstructions or factors that would affect UAV flight performance. This included indications for inclement weather, operation of other UAVs, and obstacles such as power lines, trees, equipment, and people. The UAV, including its propellers, camera, and batteries, was inspected for scratches, dents, or any other indication of flight-compromising damage. Three fully charged batteries were packed along for each site visit to ensure multiple flights could be completed. A fully charged battery and a wiped 64 GB microSD card were inserted into the UAV to complete flight preparation. The size of microSD card needed depends on how many photos will be taken during the flight and how often the photos are transferred to another storage device. Within the DJI GS Pro app, a series of system checks must pass before takeoff is allowed. This includes a Wi-Fi connection to the aircraft, GPS and IMU calibration, a battery connection, gimbal calibration, camera initialization, an SD card connection, end-of-mission action, and a transmission of the pre-flight plan waypoints. Once all tests have passed, the autonomous flight began.

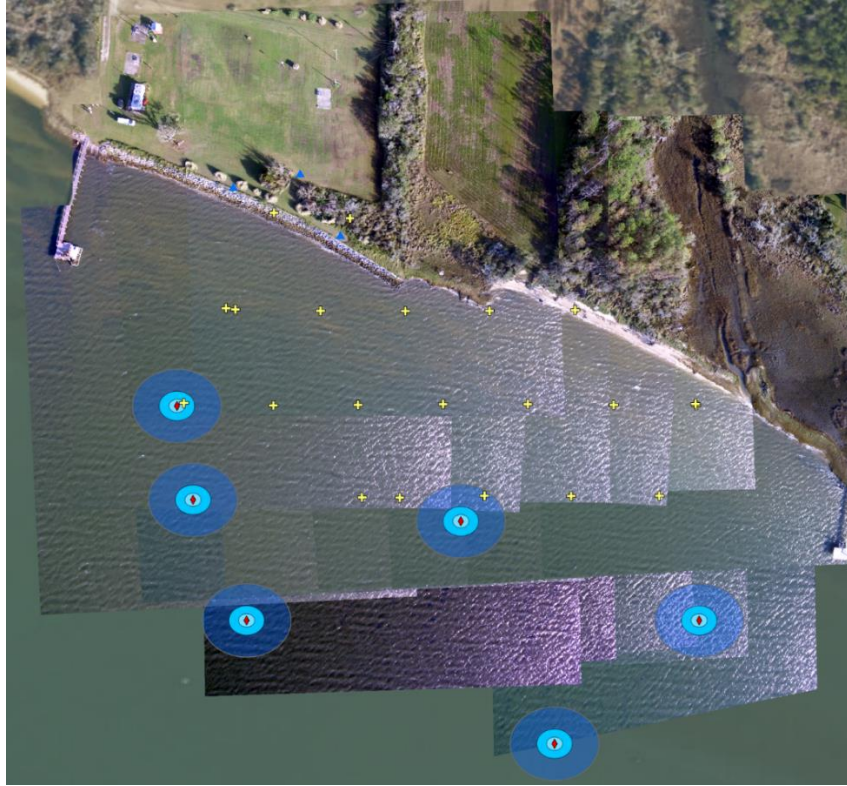
While the UAV performed the mission, line-of-sight inspection was maintained to ensure proper execution. These flights generally took around 4 minutes to complete, ending in a manual landing. Each flight was performed at 100 m AGL and at 5 m/s. With a high image overlap and a 1.66-hectare study area, waypoints are close together meaning a higher UAV speed is not necessary to complete the mission given battery and time constraints. After each flight, the microSD card was removed from the UAV and the images were duplicated and placed in a secure folder. Flight data was also downloaded from the DJI GS Pro app. Collected images and flight data were briefly reviewed to ensure quantity and quality. If the images or flights were compromised, another flight would take place.

### 3.2.2 UAV Image Analysis Procedure

UAV images for each separate data collection date were compiled together and imported into ArcGIS Pro (version 2.6.2, Redlands, California). Images that did not contain any

grab sampling points were eliminated from the data set. Due to challenges in stitching imagery over constantly moving water, images were imported individually into ArcGIS. Images containing all GCPs were then resized to the true size of each image based on the GSD, positioned using camera locations provided by the UAV, and georeferenced using the GCPs. The remaining images to be positioned do not contain any GCPs but using lease markers and other physical markers from the GCP corrected images, they can still be positioned. Each image was georeferenced using a minimum of 3 control points.

Sampling points from manual grab sampling were added to ArcGIS Pro, along with circular buffers with a radius of nine, twenty, and fifty feet. A nine-foot buffer was chosen because it was the most accurate position measurement obtained using the handheld GPS. A fifty-foot buffer was chosen because it is roughly half the distance of the resolution of the Landsat 8 satellite images described in Section 3.3.1. A sample set of camera location reference points, GCPs, sampling points, and georeferenced images can be shown in Figure 11.



◆ - Sampling Point      ● - Buffer      + - Camera Location      ▲ - GCP

**Figure 11. Reference camera locations, GCPs, sampling control points, and georeferenced images in ArcGIS Pro**

After importing and georeferencing all images from a dataset, the images were added to two custom ArcGIS Pro workflows, the first being a custom raster function and the second being a the ModelBuilder tool function (Figures 12 and 15, respectively).

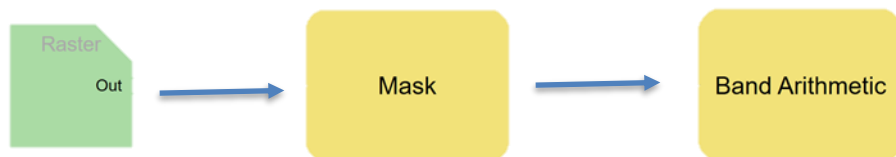


**Figure 12. Custom raster function workflow to mask and apply indices to the UAV images.**

The custom raster function first applies a mask to remove areas with high reflection within the image. It is important to mask out high sun reflectance as this could cause an overestimation of our index values. Pixels that were deemed to be within the high reflectance criteria were those that had values above 140 for every RGB band. This threshold was determined observationally by experimenting to see if all high reflectance points were accurately eliminated with the lowest possible RGB value thresholds. This process was also able to remove lease markers, which were PVC poles. The images in Figure 13 show the effects from removing the high reflectance pixels by applying the mask.

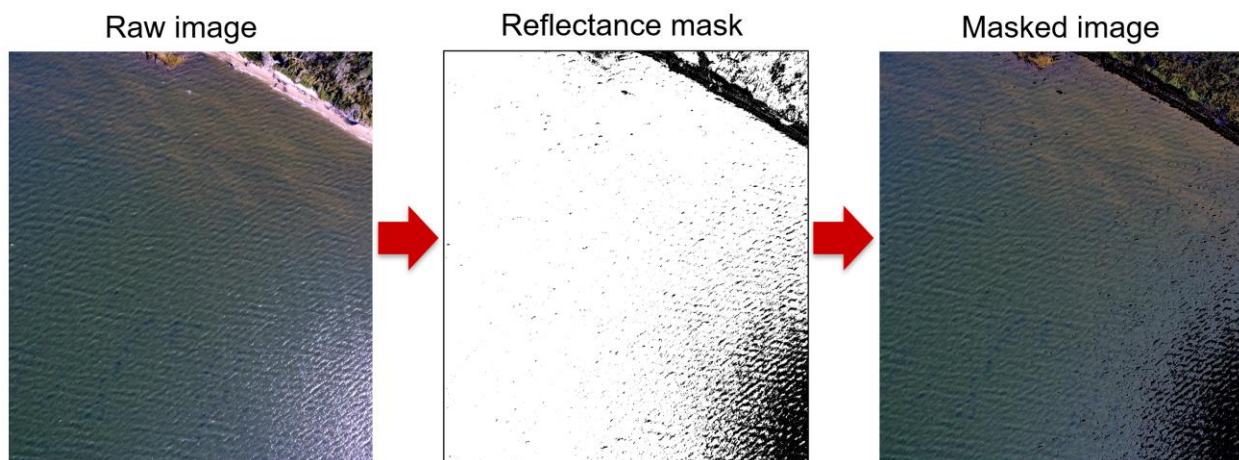


**Figure 13. Applying a mask to remove high sun reflectance and lease markers.**

Within the same function, the Band Arithmetic tool applied the specific index, whether it be ExG, RAVI, or nRAVI (equations shown in Figure 14). These three indices were chosen primarily due to their success rates in comparison to satellite imagery and extraction techniques presented in the study by Candido et al. (2016). All three indices were calculated for each included UAV image. The application of indices to a masked image within the custom raster function are shown in Figure 14.

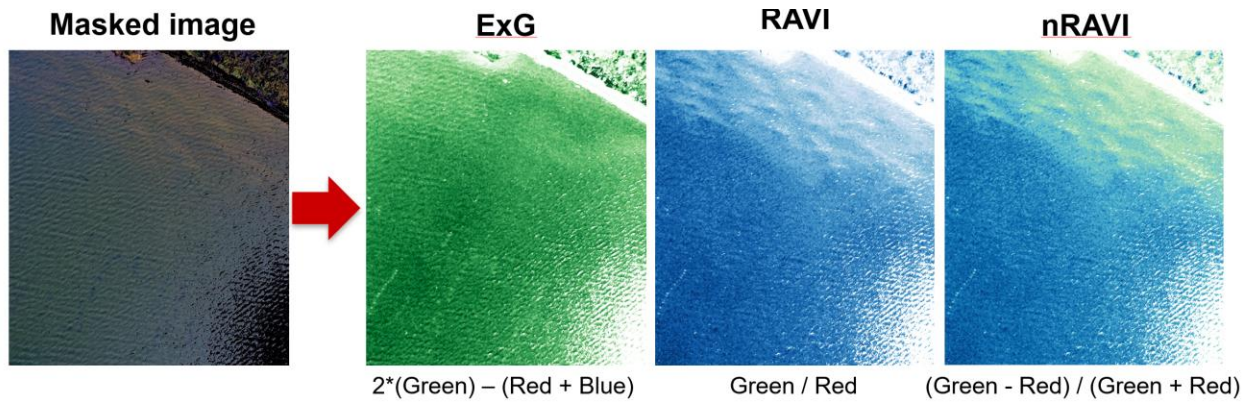


**Figure 14. Selected indices applied to a masked image with index equations below.**

The second workflow was designed to calculate zonal statistics on the masked and indexed images for each of the three buffers. This workflow is shown in Figure 15 with the buffer size parameters shown in the left blue bubbles, the index parameters in the right blue bubbles, the Zonal Statistics as Table functions in the yellow rectangles, and the resulting tables in the green bubbles.

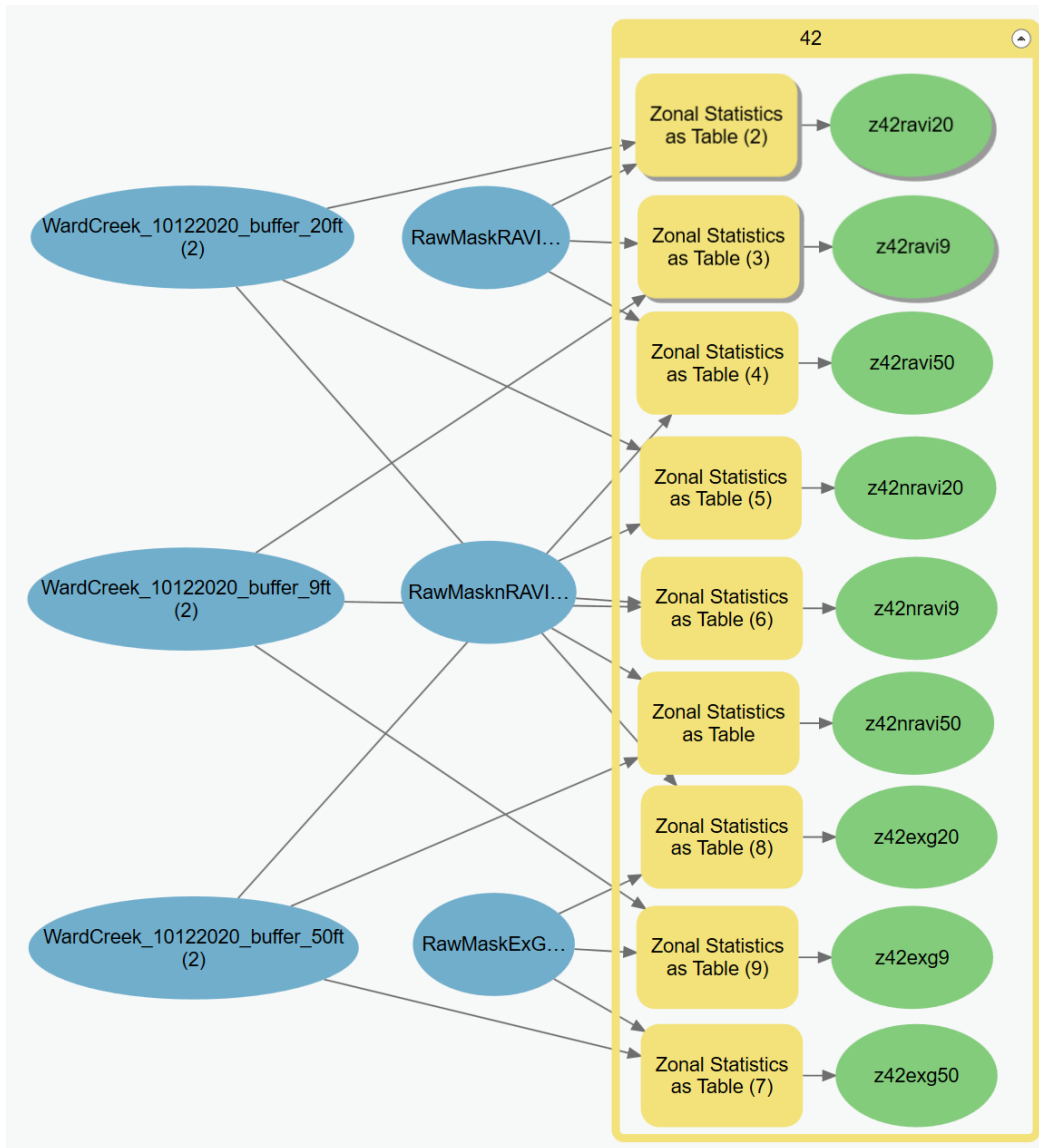


**Figure 15. Model within ArcGIS Pro to produce zonal statistics tables for each image based on index type and buffer size.**

This produced the averaged index value contained within each buffer for each sampling point. This value is what is used in correlation to the true chl-a concentrations measured through sampling and extraction.

### 3.3 Satellite Image Estimation Methods

#### 3.3.1 Satellite Imagery Collection

Satellite images were retrieved from EarthExplorer (United States Geological Survey, EarthExplorer, 2021). EarthExplorer is a database of satellite image files compiled by the USGS (United States Geological Survey, Landsat Missions, 2020). The images used for this study came from the Landsat 8 OLI/TIRS C1 Level-1 dataset. This means the images were taken from the Landsat 8 satellite, which operates with an Operational Land Imager (OLI) and Thermal Infrared Sensor (TIRS). The Level-1 data product underwent a systematic terrain correction, meaning the images were radiometrically calibrated with systemic geometric corrections applied using the spacecraft ephemeris data and DEM data to correct for relief displacement (United States Geological Survey, Landsat Level-1 Processing Details, 2020). This dataset contains a GeoTiff file containing all spectral bands as raster images produced by the Landsat 8 satellite. The bands necessary for this procedure are described in Table 5.

**Table 5. Description of spectral bands captured by the Landsat 8 satellite used for satellite estimation of chlorophyll-a.**

<b>Bands</b>	<b>Wavelength (micrometers)</b>	<b>Resolution (meters)</b>
Band 2 – Blue	0.45 – 0.51	30
Band 3 – Green	0.53 – 0.59	30
Band 4 – Red	0.64 – 0.67	30
Band 5 – Near Infrared (NIR)	0.85 – 0.88	30

### 3.3.2 Satellite Image Analysis Procedure

Satellite images were also analyzed in ArcGIS Pro. The images are first inspected to determine if they are usable, meaning clouds were not covering the area of the study site. If the images clearly showed the site, the desired spectral band images (Bands 2-5) are added to ArcGIS Pro and composited using the “Composite Bands” tool. This produces a single raster image. The compiled image was then clipped to the extent of the study site using the “Clip Raster” tool. This removes all unwanted data from outside the study area. As with the UAV image analysis procedure, these images were also masked, had indices applied to them, and the areas beneath the sampling point buffers were averaged.

## 3.4 Manual Grab Sampling

### 3.4.1 Grab Sampling Protocols

In addition to UAV surveys, six 1 L water samples were collected from across the site on each day of imaging. Sampling locations were chosen such that the points were distributed and spread out around the lease perimeter; due to physical sampling challenges, samples were distributed but not exactly evenly spaced. Samples were collected after the UAV flights to help reduce any hydrologic interference the kayaks have on phytoplankton concentrations. These samples were carefully collected from the waters’ surface by angling each polypropylene bottle sideways, dipping it no more than an inch below the surface perpendicular to the waves, and letting it fill completely. Samples were not taken directly over any oyster cages or other equipment that could skew the UAV estimation modelling. This was done to get a better representation of chlorophyll-a concentrations at the waters’ surface. Since the process of UAV image estimation relies on refraction, images best interpret concentrations on the surface. Once sample bottles were filled and labeled, they were immediately put in an ice-packed cooler and their collection location was marked with a Garmin GPSMAP® 60CSx handheld GPS (Garmin

Ltd., Olathe, Kansas) with an accuracy of 9 ft. All sample collection, preservation, and handling procedures were done according to the Florida Department of Environmental Protection Field FS 2100 standard operating procedure (FDEP 2017). To avoid degradation, the samples were temperature-maintained and kept out of sunlight since chlorophyll is sensitive to both light and heat (FDEP 2010). The samples were then transported to the lab, where they were stored in a controlled refrigerator before the extraction process.

### 3.4.2 Sample Analysis

A spectrophotometer operated in accordance with the Florida Department of Environmental Protection BB-29-1.2 standard operating procedure (FDEP 2010) provided the true concentration of chlorophyll-a at each sampled point. Briefly, 500 mL of each sample was filtered using a glass fiber filter and a vacuum filtration system to capture the phytoplankton. During the filtering process, two mL of  $\text{MgCO}_3$  suspension was added. The filter contents were then ground up with three to five mL of an aqueous acetone- $\text{MgCO}_3$  solution and placed in centrifuge tubes to be placed in the freezer overnight. The samples were centrifuged at 2500 rpms for fifteen minutes and then were decanted to remove any filter material. The samples were then placed in the spectrophotometer. The spectrophotometer used in analysis was the Thermo Scientific GENESYS 10S UV-Vis Spectrophotometer (Madison, WI, USA), which has a 1.8 nm resolution. Absorbance at wavelengths 630, 647, 664, 665, and 750 nm were recorded for each sample, along with volume filtered and volume extracted. These values are used to calculate pheophytin-corrected chl-a ( $\mu\text{g/L}$  or  $\text{mg/m}$ ). Pheophytin is a natural degradation product of chlorophyll with similar absorption peaks as chlorophyll-a. Pheophytin can often lead to the overestimation of chl-a concentrations, which is why the pheophytin-corrected chl-a concentration equation is used. Equation 1 below contains the formula contained within the FDEP BB-29-1.2 procedure for determining the corrected chl-a concentration:

$$\text{Chlorophyll } a \text{ corrected } \left( \frac{\text{mg}}{\text{m}^3} \right) = \frac{26.7(664\text{nm} - 665\text{nm}) * V_1}{V_2 * L}$$

where  $V_1$  is the volume of extractant (mL),  $V_2$  is the volume of sample filtered (L), and  $L$  is the path length (cm). Typical values of  $V_1$  ranged from eight to twelve mL and  $V_2$  ranged from 0.490 L to 0.510 L. The path length of the cuvette ( $L$ ) was one cm.

## Chapter 4 – Results

### 4.1 Summary of Data

The collection and processing of UAV imagery, satellite imagery, and surface grab samples provided data necessary to complete the objectives in Section 1.5. This section outlines the raw and processed data obtained from each of these marine chl-a estimation methodologies.

#### 4.1.1 Sample Analysis

Collected samples were analyzed by spectrophotometry for their chl-a concentration. Each sample had sampling date and sampling point ID (A-F). Quantitative data for sample analysis included volume filtered, volume of extractant, and absorption values at wavelengths of 630nm, 647nm, 664nm, 665nm, and 750nm. The results from successful sample analysis are in Appendix B.

#### 4.1.2 Satellite Imagery

Satellite image estimation was unable to be fulfilled. Each day of the study, which is the same day the Landsat 8 satellite takes images of the area, produced satellite images unfit for evaluation. Clouds completely covered the site; therefore, a comparison on the accuracy of satellite imagery and UAV RGB imagery estimation of chl-a was not completed.

#### 4.1.3 UAV RGB Imagery

The bulk of data processed came from the RGB images collected by the UAV. Categorical data for this analysis included date of collection, image ID, sampling point ID (A-F), and buffer size (9ft, 20ft, and 50ft). Preprocessing quantitative data included sampling location, ground control point location, and UAV camera location (Appendix A). Postprocessing data

included sample chl-a concentrations and average index values. A sample of tabular data after image and sample processing is shown in Table 6, and the full table is included in Appendix C.

**Table 6. Sample of tabular data from UAV image processing and extraction analysis**

Date	Image ID	Point	Buffer (ft)	True chl-a (mg/m <sup>3</sup> )	ExG	nRAVI	RAVI
10/12/2020	15	A	9	0.523529	8.724527	0.001833	1.003711
10/12/2020	16	A	9	0.523529	6.682643	0.001649	1.003344
10/12/2020	17	A	9	0.523529	5.395397	0.002241	1.004524
10/12/2020	29	A	9	0.523529	4.146752	0.023293	1.047797
10/12/2020	30	A	9	0.523529	7.410019	0.022559	1.046251
10/12/2020	31	A	9	0.523529	8.187381	0.015745	1.032107

Since there was a high UAV horizontal and vertical image overlap (80%), there were several images that provided data for the same sampling point buffer zones. Images were included in analysis for each sampling point if they covered at least 75% of a buffer zone. Table 7 displays the means and standard deviations of each index value within each buffer zone for each sampling point.

**Table 7. Sampling points and index means and standards deviations.**

Date	Sampling Point	Buffer	# of Images	ExG Mean	ExG Std	RAVI Mean	RAVI Std	nRAVI Mean	nRAVI Std
10/12/2020	A	9	13	6.703	2.058	1.048	0.034	0.024	0.017

**Table 7. Sampling points and index means and standards deviations (continued).**

10/12/ 2020	A	20	13	6.780	1.994	1.049	0.034	0.024	0.016
10/12/ 2020	A	50	13	6.631	1.848	1.049	0.032	0.024	0.015
10/12/ 2020	B	9	11	3.480	3.891	1.049	0.022	0.024	0.011
10/12/ 2020	B	20	11	3.679	3.896	1.048	0.022	0.023	0.010
10/12/ 2020	B	50	10	4.030	3.539	1.047	0.022	0.023	0.011
10/12/ 2020	E	9	3	-1.795	3.555	1.051	0.034	0.025	0.016
10/12/ 2020	E	20	2	-3.240	3.448	1.035	0.023	0.017	0.011
10/12/ 2020	F	9	6	-0.865	6.079	1.024	0.027	0.012	0.013
10/12/ 2020	F	20	5	0.202	5.777	1.030	0.024	0.015	0.011
10/12/ 2020	F	50	4	1.266	5.882	1.037	0.019	0.018	0.009
11/11/ 2020	A	9	6	14.090	2.163	1.115	0.037	0.054	0.017
11/11/ 2020	A	20	6	14.093	2.111	1.115	0.038	0.057	0.019
11/11/ 2020	A	50	4	13.854	2.321	1.098	0.030	0.047	0.014

**Table 7. Sampling points and index means and standards deviations (continued).**

11/11/ 2020	B	9	6	9.642	3.541	1.081	0.038	0.039	0.018
11/11/ 2020	B	20	6	9.978	3.534	1.082	0.040	0.039	0.018
11/11/ 2020	B	50	6	9.718	3.591	1.081	0.040	0.039	0.018
11/11/ 2020	C	9	1	8.662	0	1.092	0.000	0.044	0.000
11/11/ 2020	C	20	1	8.931	0	1.093	0.000	0.044	0.000
11/11/ 2020	C	50	1	9.339	0	1.095	0.000	0.045	0.000
11/11/ 2020	E	9	1	14.484	0	1.077	0.000	0.037	0.000
11/11/ 2020	E	20	1	14.378	0	1.082	0.000	0.039	0.000
11/11/ 2020	E	50	1	13.715	0	1.082	0.000	0.039	0.000
11/11/ 2020	F	9	4	14.985	1.662	1.108	0.021	0.051	0.010
11/11/ 2020	F	20	4	14.819	1.372	1.108	0.023	0.054	0.014
11/11/ 2020	F	50	2	15.195	1.842	1.090	0.013	0.043	0.006

In Table 7, sampling points C and D for the 10/12/2020 dataset were eliminated from analysis because the sun reflectance mask eliminated enough pixels to push them under the 75% buffer zone cover threshold.

## 4.2 Regression Analysis

Several plots and models were created to explore the relationship between indices and true chl-a concentrations. These models only include buffer zones that were at least 75% encapsulated by an image after masking. The scatter plots shown in Figures 16-24 are segregated by index and buffer size and display each images' index values for each sampling point. The blue dotted line on each of these plots represent a linear regression fit with the corresponding model equation in the black box. The orange dotted lines represent a 2<sup>nd</sup> order polynomial fit with the corresponding model equation in the orange box.

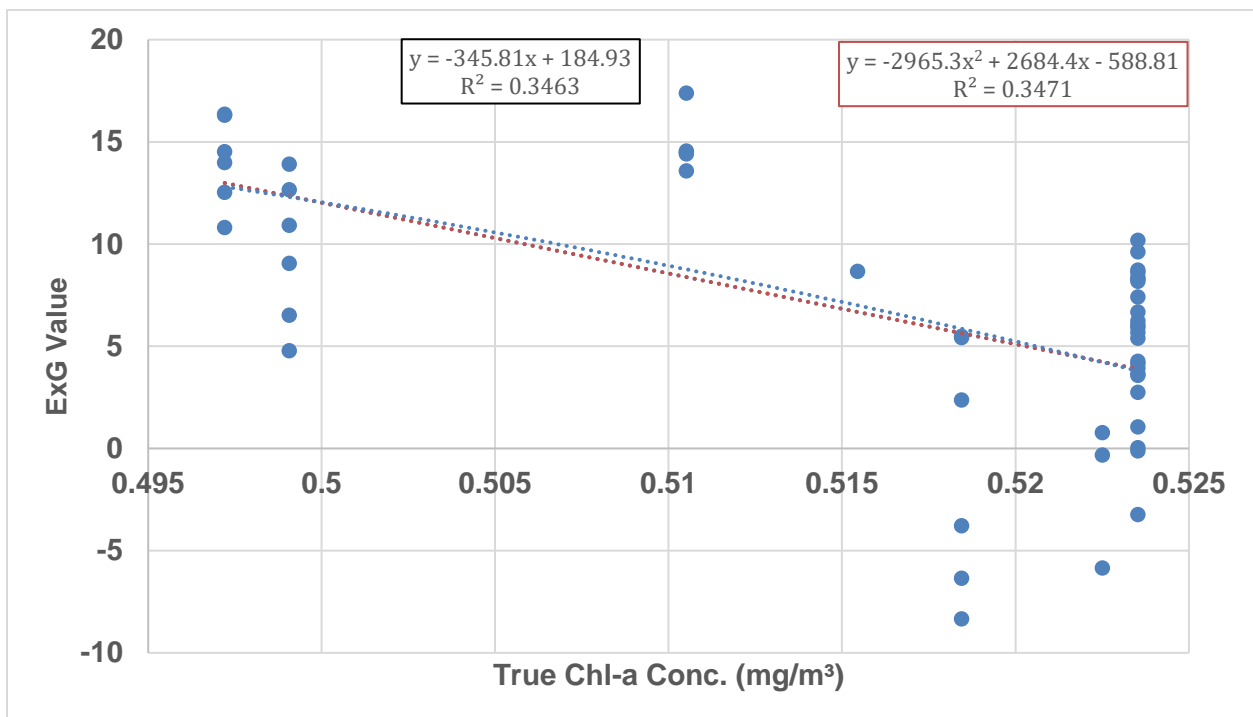


Figure 16. Average ExG values within the nine-foot buffer vs. true chl-a values from sampling and extraction for each sampled point

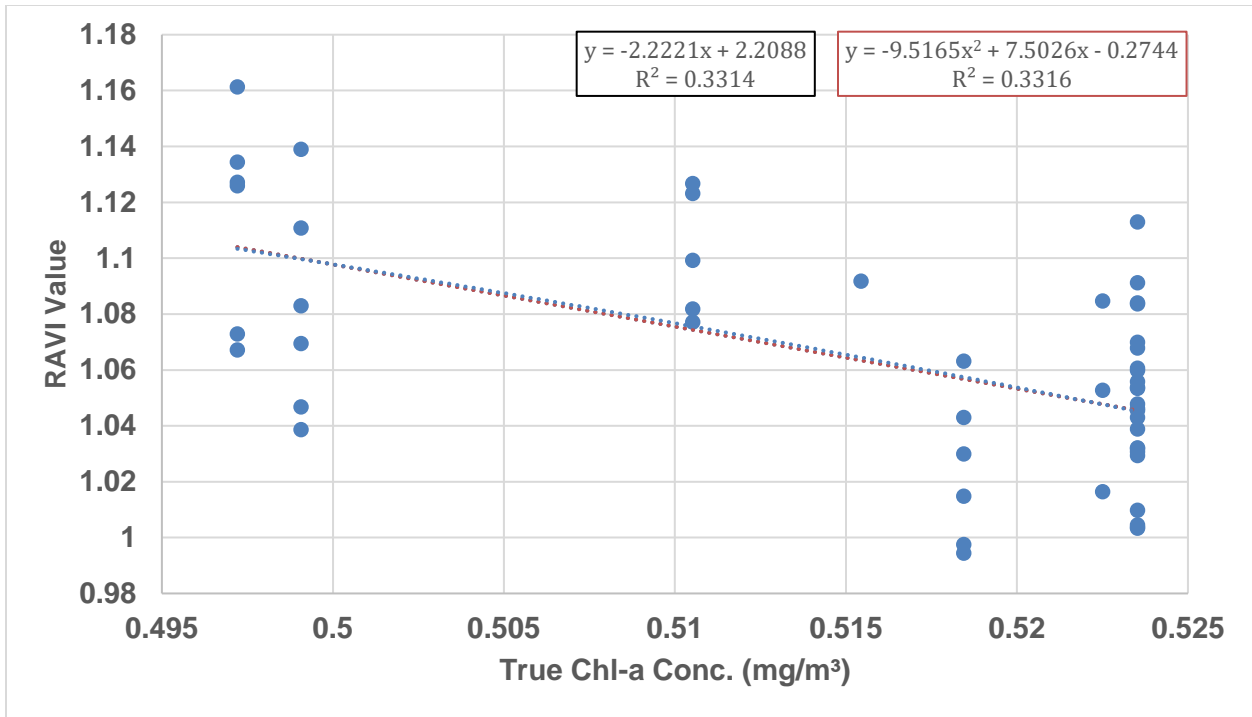


Figure 17. Average RAVI values within the nine-foot buffer vs. true chl-a values from sampling and extraction for each sampled point

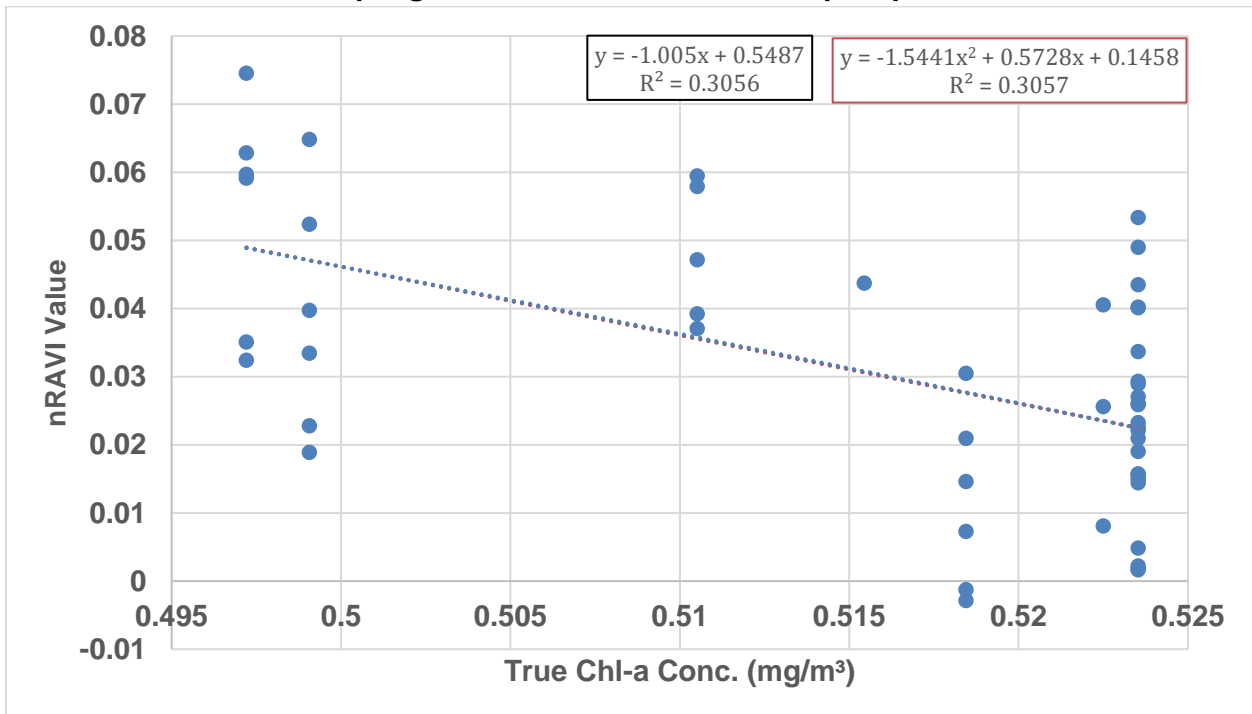


Figure 18. Average nRAVI values within the nine-foot buffer vs. true chl-a values from sampling and extraction for each sampled point

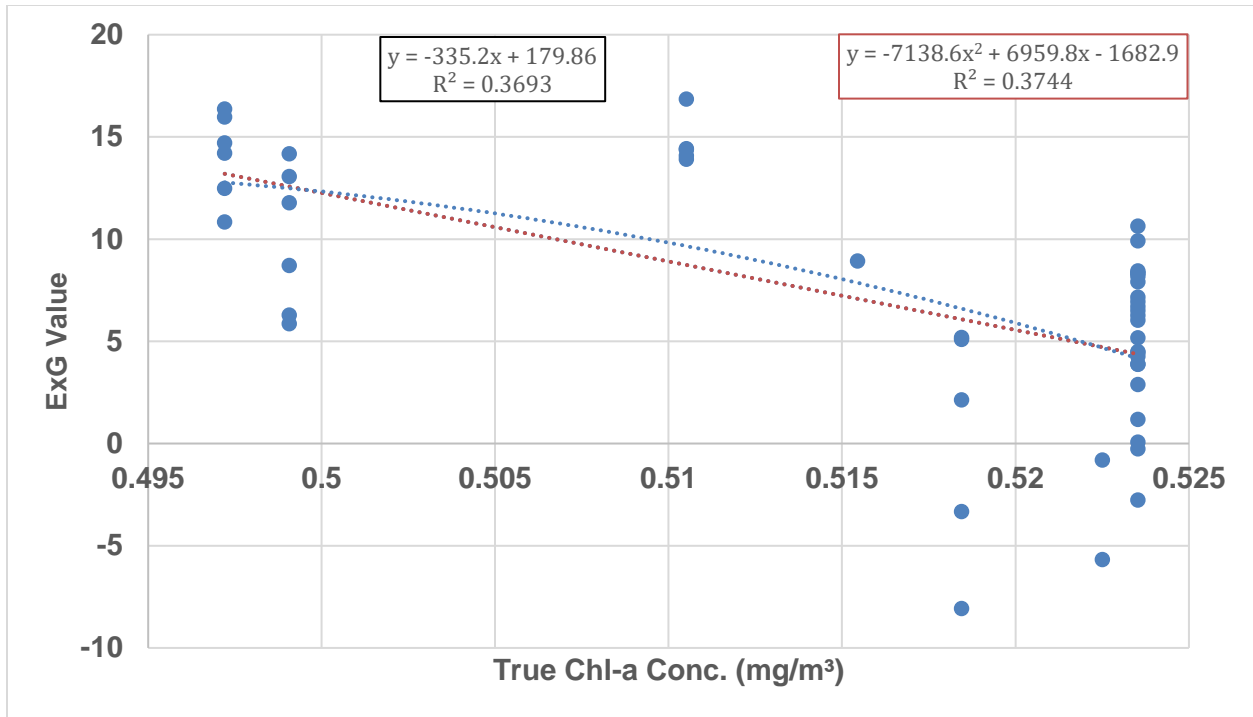


Figure 19. Average ExG values within the twenty-foot buffer vs. true chl-a values from sampling and extraction for each sampled point

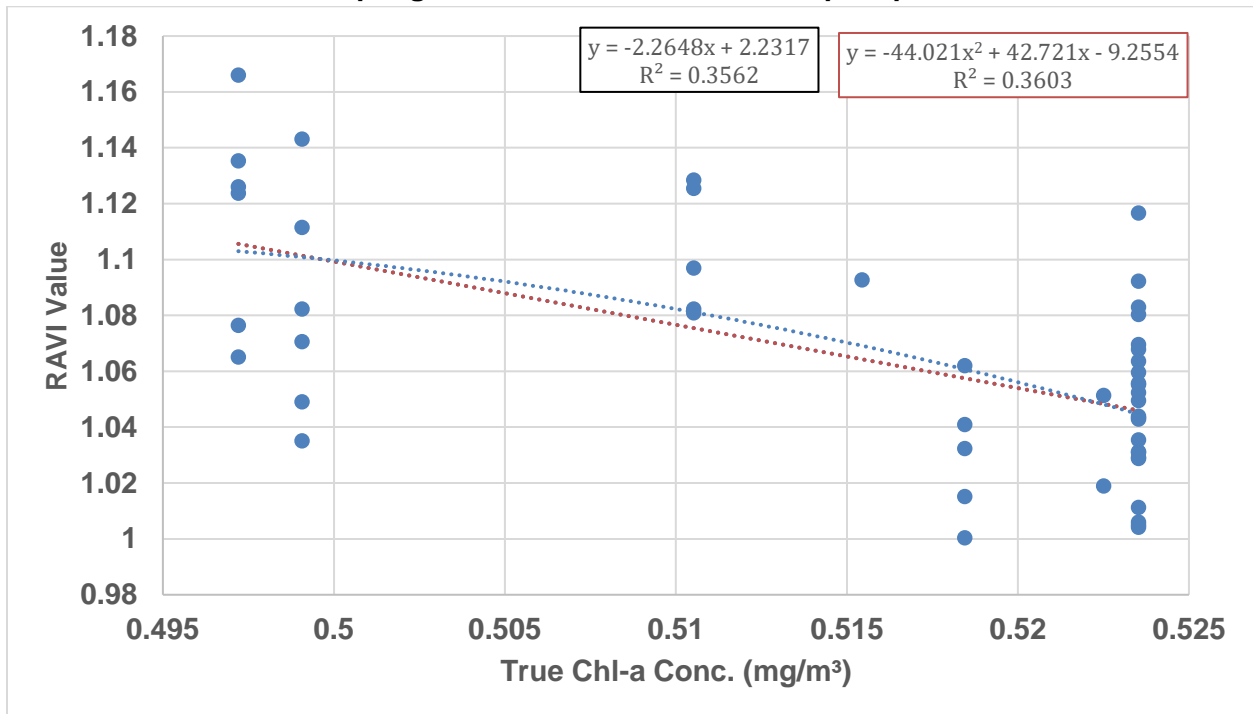


Figure 20. Average RAVI values within the twenty-foot buffer vs. true chl-a values from sampling and extraction for each sampled point

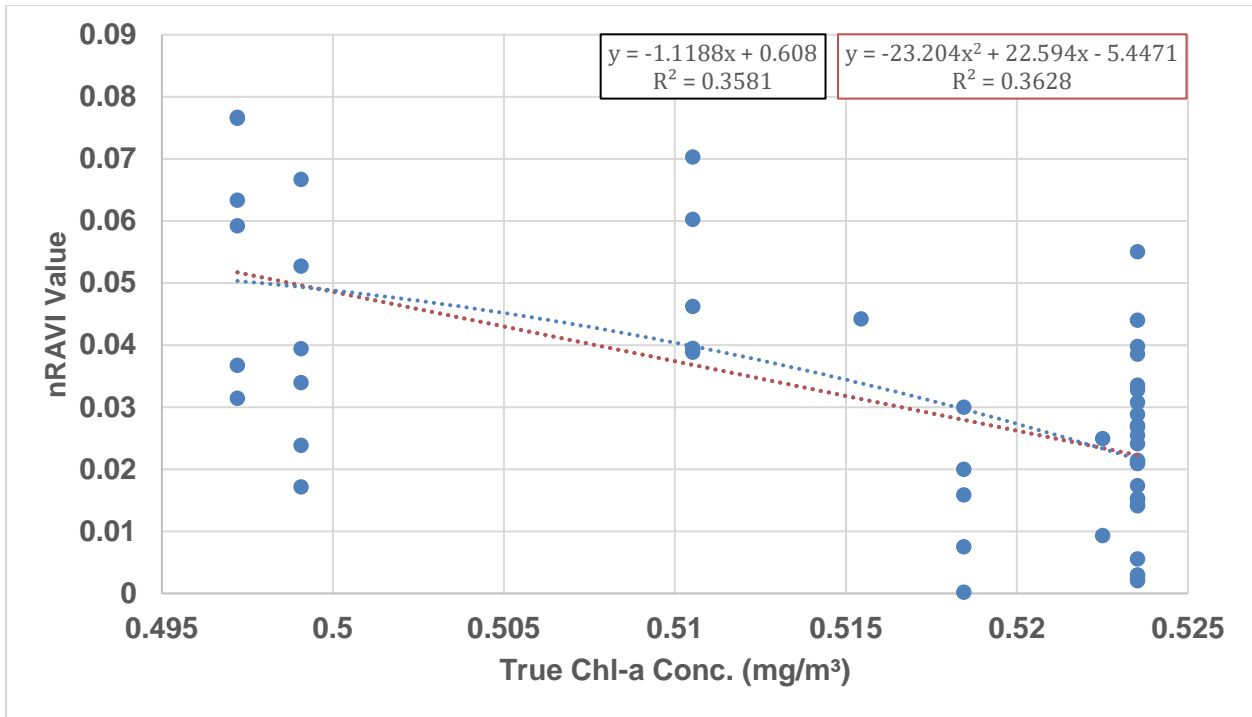


Figure 21. Average nRAVI values within the twenty-foot buffer vs. true chl-a values from sampling and extraction for each sampled point

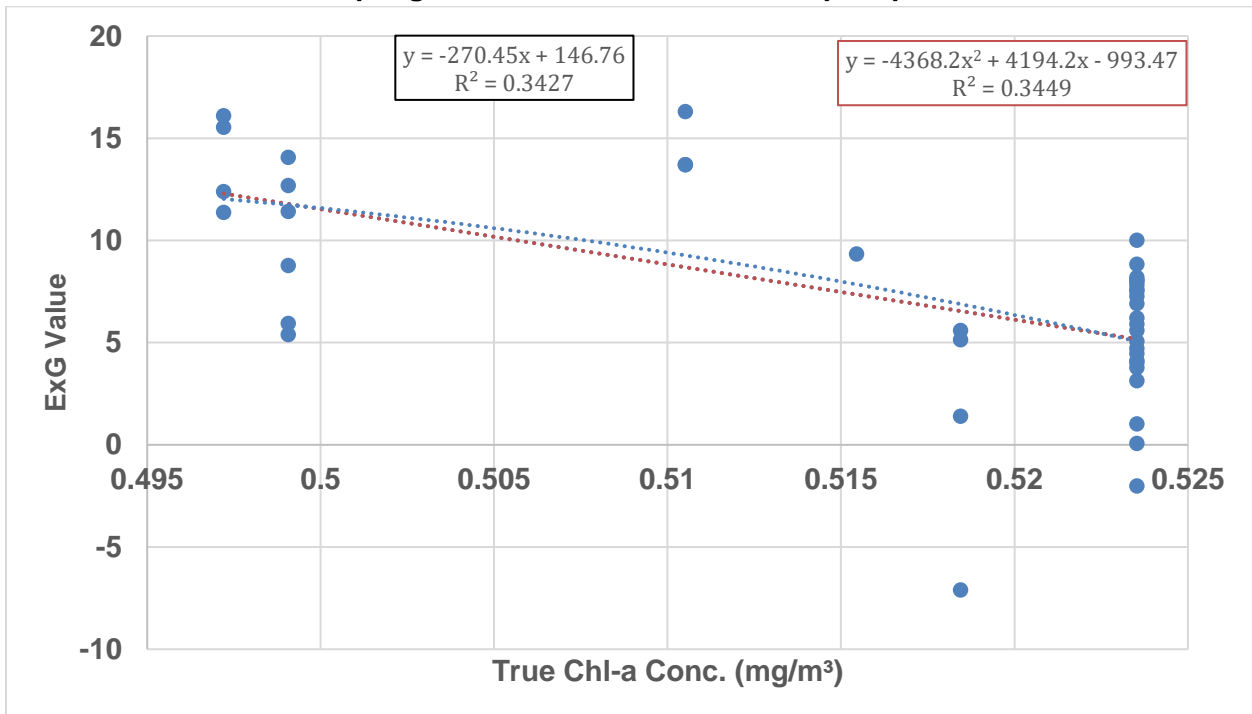


Figure 22. Average ExG values within the fifty-foot buffer vs. true chl-a values from sampling and extraction for each sampled point

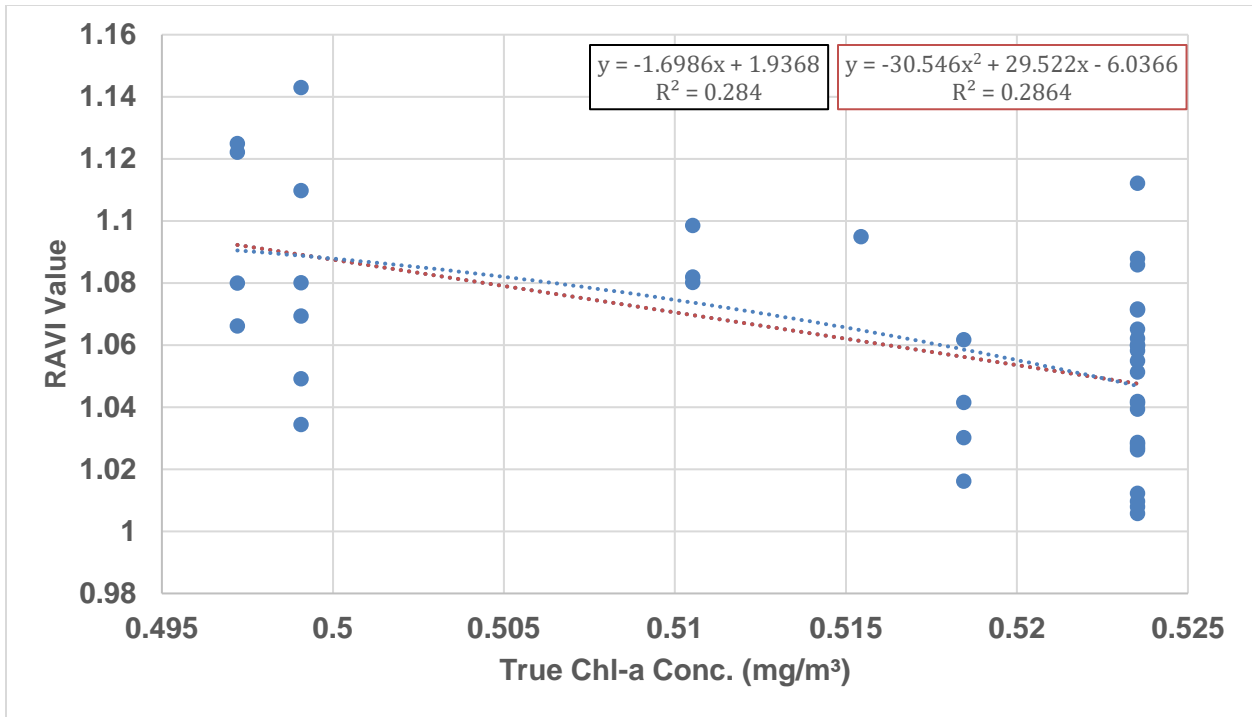


Figure 23. Average RAVI values within the fifty-foot buffer vs. true chl-a values from sampling and extraction for each sampled point

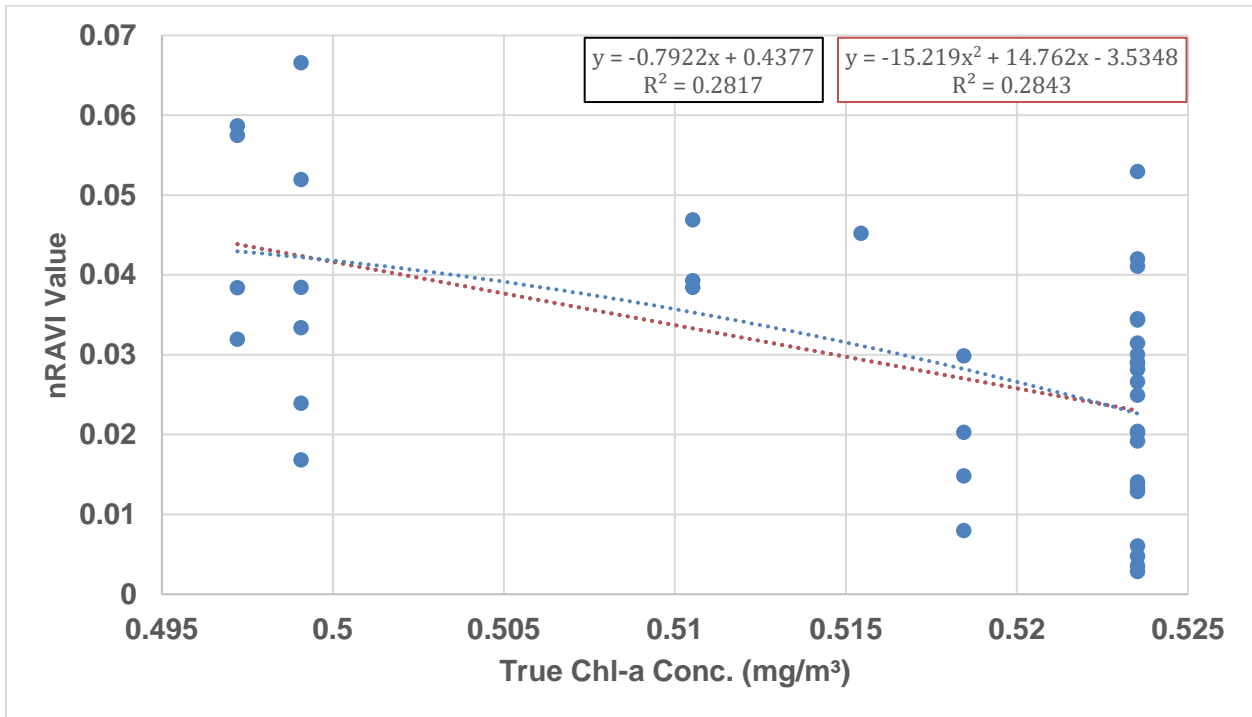


Figure 24. Average nRAVI values within the fifty-foot buffer vs. true chl-a values from sampling and extraction for each sampled point

These model equations represent the relationship of the true chl-a concentration and the produced index value. In all of these model equations, there is a negative relationship, so as true chl-a concentration increases, the index value typically decreases.

Linear, multilinear, quadratic, and multiquadratic regression models were created for each buffer size. Multilinear and multiquadratic models were composed of a combination of indices, meaning the models had two or three dependent variables. The regression equations along with resulting multiple R values, coefficients of correlation, adjusted coefficients of correlation, standard errors, root mean square error, and number of observations are listed in Appendix E. The top five best performing models according to adjusted coefficient of correlation are shown in Table 8. The other models and their multilinear regression formulas are also listed in Appendix E.

**Table 8. Top performing models (adjusted R<sup>2</sup>)**

<b>Model</b>	<b>Regression Formula</b>	<b>Adjusted R<sup>2</sup></b>
ExG+nRAVI (20ft)	$Y = -0.00067*ExG - 0.1794*nRAVI + 0.52568$	0.399
ExG+RAVI (20ft)	$Y = -0.00067*ExG - 0.08728*RAVI + 0.613567$	0.399
ExG+nRAVI+RAVI (20ft)	$Y = -0.00066*ExG - 0.09427*nRAVI - 0.04265*RAVI + 0.568389$	0.387
ExG+nRAVI+RAVI (9ft)	$Y = -0.00061*ExG + 0.636799*nRAVI - 0.38157*RAVI + 0.90582$	0.383
ExG+RAVI (9ft)	$Y = -0.00062*ExG - 0.08336*RAVI + 0.608235$	0.374

More statistical information regarding these top performing models are displayed in Table 9.

**Table 9. Top performing models' coefficients of correlation, standard error, and number of observations**

<b>Index</b>	<b>Multiple R</b>	<b>R<sup>2</sup></b>	<b>Adjusted R<sup>2</sup></b>	<b>Standard Error</b>	<b>Observations</b>
ExG+nRAVI (20ft)	0.651	0.424	0.399	0.008	49
ExG+RAVI (20ft)	0.651	0.424	0.399	0.008	49
ExG+nRAVI+RAVI (20ft)	0.652	0.425	0.387	0.008	49
ExG+nRAVI+RAVI (9ft)	0.648	0.420	0.383	0.008	51
ExG+RAVI (9ft)	0.632	0.399	0.374	0.008	51

P-values, as an indicator for statistical significance, for each variable (index) in these top-performing models are displayed in Table 10.

**Table 10. Index significance in each of the top-performing models.**

<b>Model</b>	<b>ExG P-value</b>	<b>nRAVI P-value</b>	<b>RAVI P-value</b>
ExG+nRAVI (20ft)	0.026	0.042	-
ExG+RAVI (20ft)	0.024	-	0.042
ExG+nRAVI+RAVI (20ft)	0.028	0.821	0.835
ExG+nRAVI+RAVI (9ft)	0.024	0.202	0.110
ExG+RAVI (9ft)	0.024	-	0.045

In each of these models the ExG index variable is statistically significant ( $p$ -value < 0.05). In models containing ExG and a single other index, the accompanying index is also statistically significant.

True chl-a concentrations were plotted against predicted chl-a concentrations from the linear regression analysis (Figures 25-29).

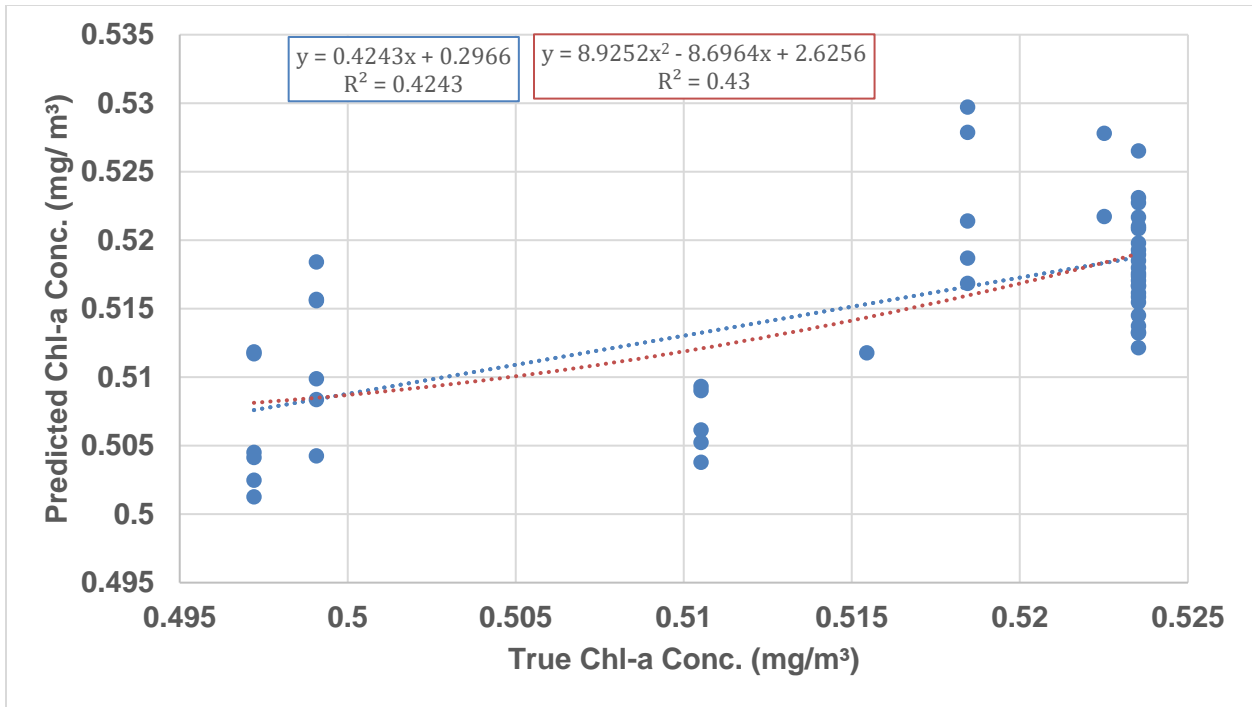


Figure 25. True vs. ExG+nRAVI (20ft) model predicted chl-a concentrations (mg/m³)

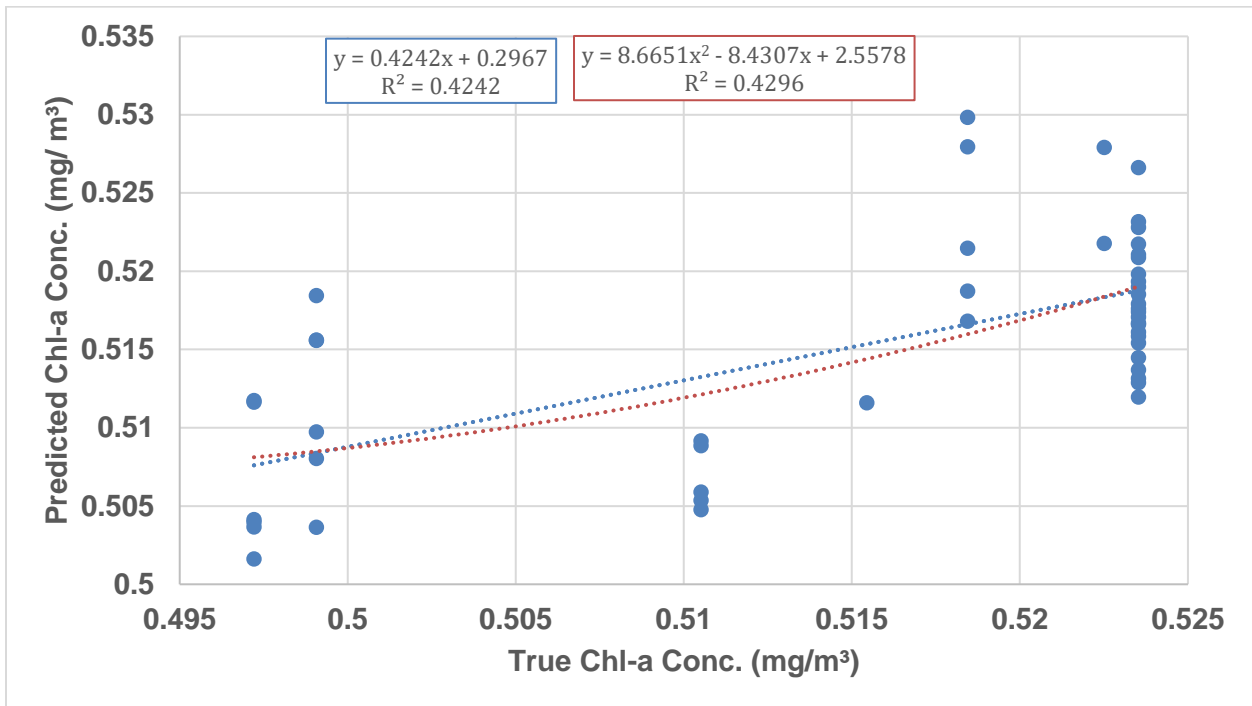


Figure 26. True vs. ExG+RAVI (20ft) model predicted chl-a concentrations (mg/m³)

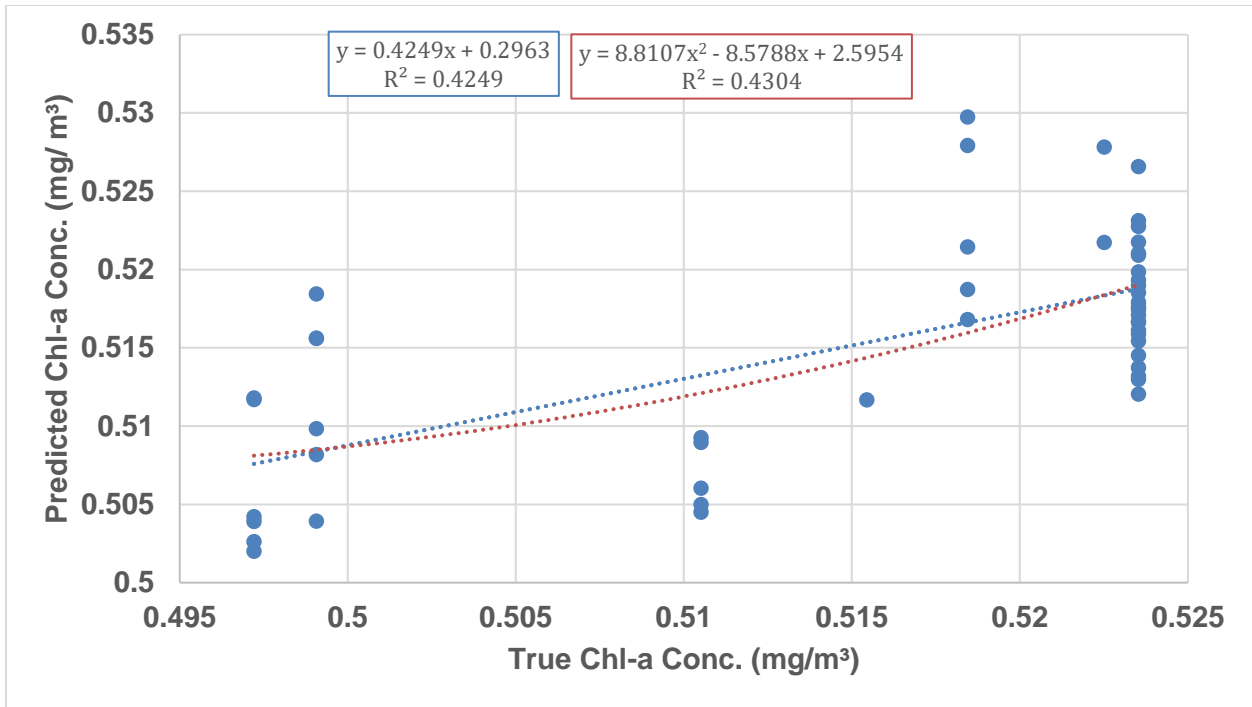


Figure 27. True vs. ExG+nRAVI+RAVI (20ft) model predicted chl-a concentrations (mg/m³)

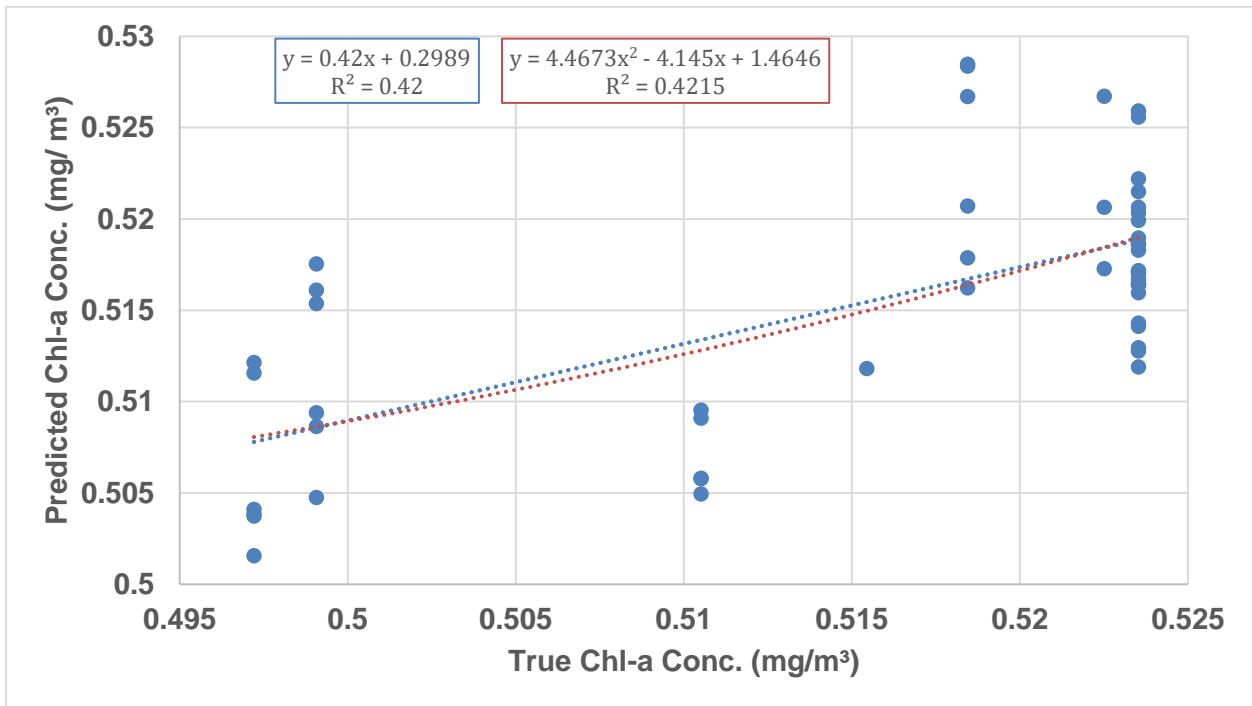
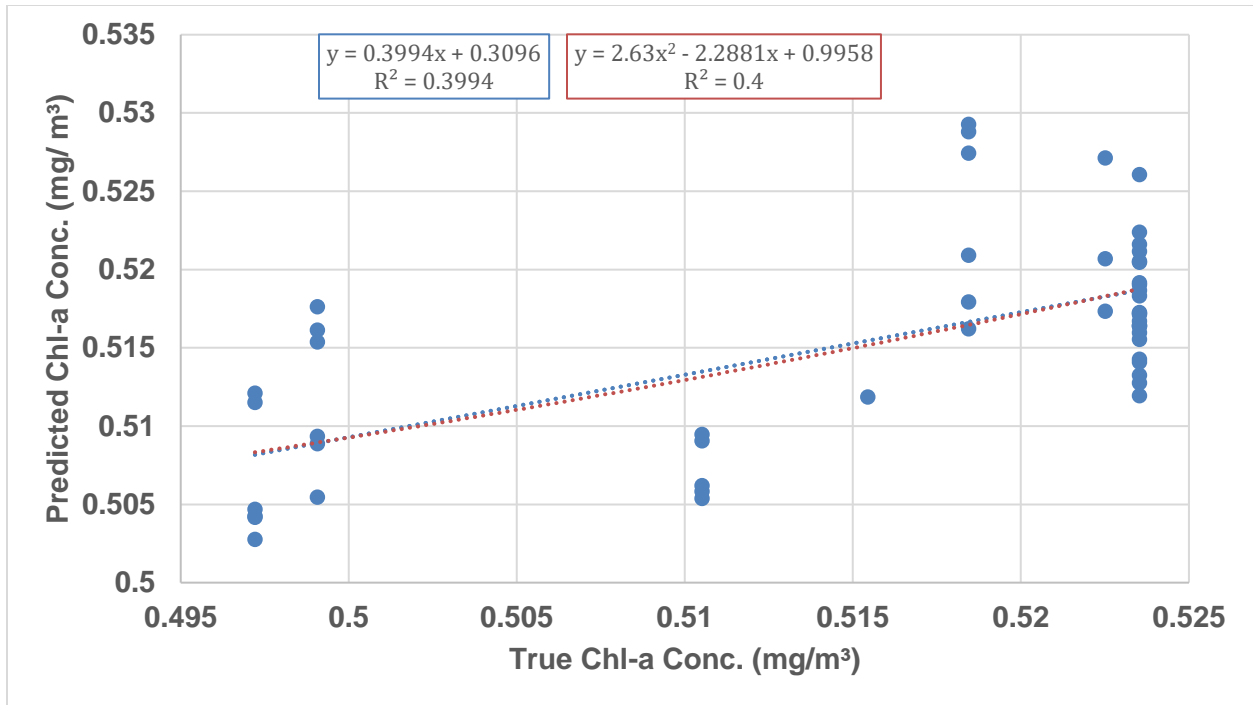


Figure 28. True vs. ExG+nRAVI+RAVI (9ft) model predicted chl-a concentrations (mg/m³)



**Figure 29. True vs. ExG+RAVI (9ft) model predicted chl-a concentrations (mg/m<sup>3</sup>)**

Results of actual measurements of chl-a were compared with predictive models based on UAV RGB imaging to assess statistical significance and R-squared fit for each index and buffer size models. Several models including ExG, RAVI and nRAVI were significant in their correlations at all buffer sizes, except the nRAVI+RAVI models. Further discussion on the meaning and possible implications of these findings will be discussed in the following section.

# Chapter 5 – Discussion

## 5.1 Model Evaluation

A few interesting phenomena and limitations were observed through the resulting data, and a number of statistical and procedural techniques were used to understand and clarify this data. These include management of images and data points, use of different models, procedural critiques, and other considerations. These will be discussed in this chapter.

### 5.1.1 Removed Data Points

Data points with index value outliers that resulted in their removal from model consideration almost exclusively contained buffers with a greater number of pixels masked out due to sun reflectance. After the masking process, these pixels contained a 'NoData' value and were ignored in zonal statistic calculations. One theory as to what causes this phenomenon is the underestimation of index values due to shadows caused by waves. As highlighted in Figure 30, high reflectance is observed to primarily lie among the peaks of waves. The RGB values of these shadows may need to be categorized and another mask may need to be created.

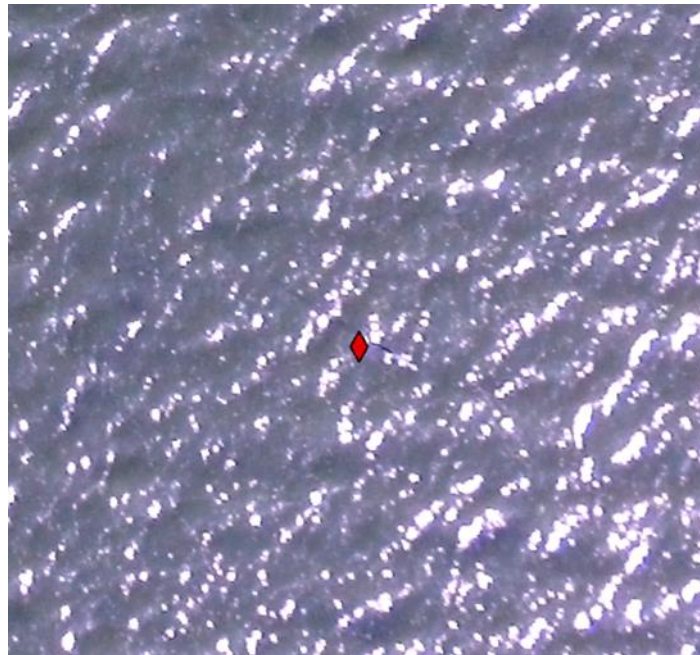


**Figure 30. High reflectance among wave peaks**

#### 5.1.2 Variability in Index Values

Referring to Table 7, standard deviations between index values of the same sampling point buffer across multiple overlapping images are fairly large. This issue could possibly be attributed to rapid changes in sun reflectance, such as with cloud cover. Hydrologic effects could also result in variability between images, considering how much of the waves peaks or troughs are contained within the buffer zones. This variation directly contributes to higher variation between model predicted and true chl-a concentrations.

#### 5.1.3 Index and Buffer Size

There are a few trends when comparing the linear and multilinear regression models. Models containing the ExG index consistently performed better than those that did not. This is consistent with the findings of the UAV RGB freshwater imaging study by Candido et al. (2016). Without the use of the NIR band, the green band seems to carry a greater significance

in the detection of chlorophyll-a. Another observation is that 20ft buffer models performed better than 9- and 50-foot buffer models. The 50ft buffer models performed the worst, possibly due to an increased chance of RGB value variability.

#### 5.1.4 Variability in Sampled Chl-a Concentrations

These models failed to be considered robust as there was very low variability in sample chl-a values across collection dates. Low variability is to be expected on a single collection date when samples are collected within minutes from each other across an area as small as two acres, but in brackish, tidal waters, a higher variability is expected across multiple sample collection days. A more robust model formulated with a higher variability in sampling concentrations could be applied to marine waters with higher chl-a concentrations, but this study could only be extrapolated to areas where concentrations are considered very low ( $<1.0 \text{ mg/m}^3$ ).

#### 5.1.5 Comparison of Estimation Method Effectiveness

While image resolution greatly increased from 30m with the Landsat 8 satellite to 0.045m with the DJI Phantom 3 Standard UAV, the accuracy of these models is not yet comparable to satellite or multispectral UAV estimation methods based on recent literature. If improvements in UAV RGB imagery models are made comparable to satellite or multispectral UAV imagery models, a greater resolution would provide insight into the hydrologic effects of phytoplankton concentrations surrounding shellfish leases.

## 5.2 Procedure Evaluation

### 5.2.1 Consideration of Time

Procedurally, if this model could be made more robust, I feel this methodology could benefit the shellfish industry as the time taken to image the site and estimate concentrations

was less than time spent sampling and analysis in the lab. Short static surveys of the area to establish ground control points took approximately 15 minutes. An initial calibration of the model using sampling and lab estimated chl-a concentrations is most likely necessary, but after a model is created, it is believed that only UAV RGB image collection and processing will be necessary in subsequent analyses. The image collection process, with the flight parameters discussed in section 3.2.1, takes about two to three minutes per acre. The time taken for image processing, using the outlined procedure and custom ArcGIS Pro functions can also take little time, especially when compared with the lab extraction process. After model creation, environments with similar conditions can utilize that model to produce quick meaningful results through the UAV imaging and processing methods alone.

#### 5.2.2 Ease of Implementation and Model Maintenance

The UAV RGB imagery procedure requires the user to know the basics of small UAV piloting, ArcGIS Pro, and a statistical analysis software, such as Microsoft Excel or R. With the development of a user-friendly step-by-step guide, the end user of the technology may not require a detailed knowledge into the specifics of these analytical procedures.

Initial and periodic manual sampling may still be required for calibration to specific sites and conditions. Periodic sampling may only be necessary if drastic or rapid changes to the site occurs. A reasonable approximation of shellfish food supply could be obtained regularly through the basics of this procedure.

# Chapter 6 – Conclusion

## 6.1 Summary

Environmental monitoring is a necessary function of modern aquaculture as it allows researchers and growers the opportunity to obtain a higher insight into the inputs and outputs of their operation. The inclusion of intelligent sensing and data analytics in aquaculture can help to improve management practices, provide better risk assessment, transform animal care, reduce waste, increase innovation and productivity, improve profits, improve supply chain management, and improve the environment. Common sampling and laboratory analysis, satellite imagery, and multispectral UAV imagery techniques have enabled shellfish growers to estimate the concentrations of phytoplankton within their leases, providing greater awareness to the amount of feed their shellfish are receiving. Due to the drawbacks of each of these methods, the work within this thesis attempted to solve some of those issues by developing a quick, safe, and reliable way to estimate marine phytoplankton concentrations with the use of UAV RGB imagery.

In conclusion, UAV imagery estimation models for marine chl-a concentrations need more experimentation to be considered robust and effective. With the ExG index included in a multivariate linear model with the RAVI or nRAVI indices at a buffer of 20ft, approximately 40% of the model variation can be explained for low marine chl-a concentrations through this methodology. Single variable models with these indices (ExG, RAVI, and nRAVI) and 9ft and 50ft models performed slightly worse. With low model accuracy in estimating marine chl-a concentrations, it is recommended that other estimation techniques be performed to better estimate concentrations.

## 6.2 Suggestions for Future Work

Future work could include exploration into many parts of the UAV RGB image estimation process. To eliminate errors in sampling, automation using uncrewed surface vehicles could help to reduce potential human error in sample collection GPS positioning as well as assist in water-dominated image stitching to provide a single image of a site. Since there were extremely low chl-a concentrations and low variability within this study, trials in marine areas with a higher variability of phytoplankton concentrations or simply more sampling will help to improve upon the robustness of this technique. The addition of a variety of non-image-based water quality parameters could help to improve these models by accounting for broader physical/biochemical effects on phytoplankton concentrations. It is also recommended that laboratory analysis include manual cell counting or flow cytometry to test the accuracy of spectrophotometric determination of chl-a concentrations.

Within image analysis, other indices and modelling techniques should be explored. Machine learning could help to automate analytical model building by learning from vast amounts of data and identifying patterns within these UAV images. With several images having to be removed from these datasets, simply more data could be collected to remove any large effects from any data outliers.

## References

- Al-Wassai, F. A., & Kalyankar, N. V. (2013). Major limitations of satellite images. *arXiv preprint arXiv:1307.2434*.
- Babin, M., Roesler, C. S., & Cullen, J. J. (2008). *Real-time coastal observing systems for marine ecosystem dynamics and harmful algal blooms: Theory, instrumentation and modelling*. Unesco.
- Blondeau-Patissier, D., Gower, J. F., Dekker, A. G., Phinn, S. R., & Brando, V. E. (2014). A review of ocean color remote sensing methods and statistical techniques for the detection, mapping and analysis of phytoplankton blooms in coastal and open oceans. *Progress in oceanography*, 123, 123-144.
- Cândido, A. K. A. A., Paranhos Filho, A. C., Haupenthal, M. R., da Silva, N. M., de Sousa Correa, J., & Ribeiro, M. L. (2016). Water quality and chlorophyll measurement through vegetation indices generated from orbital and suborbital images. *Water, Air, & Soil Pollution*, 227(7), 224.
- Chen, T. (2021, April 1). *How to become data-driven in aquaculture*. The Fish Site. <https://thefishsite.com/articles/how-to-become-data-driven-in-aquaculture>.
- Costa, J. P., & Rihtar, M. (2016). Data Analytics in Aquaculture.
- Cullen, J. J. (1982). The Deep Chlorophyll Maximum: Comparing Vertical Profiles of Chlorophyll a. *Canadian Journal of Fisheries and Aquatic Sciences*, 39(5), 791–803. <https://doi.org/10.1139/f82-108>
- Decker, C., & Simmons, K. (2013). Surface Water Sampling. *U.S. Environmental Protection Agency Science and Ecosystem Support Division*, (SESDPROC-201-R3).
- Dickey, T., Lewis, M., & Chang, G. (2006). Optical oceanography: recent advances and future directions using global remote sensing and in situ observations. *Reviews of geophysics*, 44(1).
- Dore, J. E., Letelier, R. M., Church, M. J., Lukas, R., & Karl, D. M. (2008). Summer phytoplankton blooms in the oligotrophic North Pacific Subtropical Gyre: Historical perspective and recent observations. *Progress in Oceanography*, 76(1), 2–38. <https://doi.org/10.1016/j.pocean.2007.10.002>
- Duncan, P. F. (2003). Shellfish: Commercially Important Molluscs.
- Environmental Protection Agency. (2013). Standard Operating Procedure for Chlorophyll a Sampling Method Field Procedure, *Revision 07*.

- Environmental Protection Agency. (2016, August 16). *Indicators: Chlorophyll a*. National Aquatic Resource Surveys.
- European Environment Agency. (2021, May 11). *Chlorophyll in transitional, coastal and marine waters*. <https://www.eea.europa.eu/data-and-maps/indicators/chlorophyll-in-transitional-coastal-and-3/assessment>.
- Faust, M. A., & Norris, K. H. (1985). In vivo spectrophotometric analysis of photosynthetic pigments in natural populations of phytoplankton. *Limnology and Oceanography*, 30(6), 1316–1322. <https://doi.org/10.4319/lo.1985.30.6.1316>
- Food and Agriculture Organization. 2020. The State of World Fisheries and Aquaculture 2020 - Sustainability in Action. Rome. Licence: CC BY-NC-SA 3.0 IGO.
- Florida Department of Environmental Protection (2010). Standard Operating Procedure for: Spectrophotometric Determination of Corrected and Uncorrected Chlorophyll a and Pheophytin. Department of Environmental Protection Bureau of Laboratories Biology Section, Tallahassee Florida.
- Florida Department of Environmental Protection (2017). Standard Operating Procedure for: Surface Water Sampling. Department of Environmental Protection.
- Franklin, J. B., Sathish, T., Vinithkumar, N. V., & Kirubakaran, R. (2020). A novel approach to predict chlorophyll-a in coastal-marine ecosystems using multiple linear regression and principal component scores. *Marine Pollution Bulletin*, 152, 110902.
- Gitelson, A. A., Dall'Olmo, G., Moses, W., Rundquist, D. C., Barrow, T., Fisher, T. R., Gurlin, D., & Holz, J. (2008). A simple semi-analytical model for remote estimation of chlorophyll-a in turbid waters: Validation. *Remote Sensing of Environment*, 112(9), 3582-3593.
- Green, D. R., Hagon, J. J., Gómez, C., & Gregory, B. J. (2019). Using Low-Cost UAVs for Environmental Monitoring, Mapping, and Modelling: Examples from the Coastal Zone. *Coastal Management, Global Challenges and Innovations*, 465–501. <https://doi.org/10.1016/b978-0-12-810473-6.00022-4>
- Gregor, J., Geriš, R., Maršálek, B., Heteša, J., & Marvan, P. (2005). In situ quantification of phytoplankton in reservoirs using a Submersible Spectrofluorometer. *Hydrobiologia*, 548(1), 141–151. <https://doi.org/10.1007/s10750-005-4268-1>
- Gupta, S. (2018, May 28). *Data Science in the Indian Agriculture Industry*. Analytics Vidhya. <https://www.analyticsvidhya.com/blog/2018/05/data-analytics-in-the-indian-agriculture-industry/>
- Hall, S. G., Campbell, M., Geddie, A., Thomas, M., Paul, D., Wilcox, D., Smith, R., Eddy, N., Frinkso, M., Wilder, S., Doman, K., Smith, D., Traenkle, J., & Kelly, R. (2018).

- Engineering Challenges in Marine Aquaculture. In *2018 ASABE Annual International Meeting*. American Society of Agricultural and Biological Engineers.
- Helmstetter, M. (2019, April 4). The Aquaculture Industry: An Ocean Of Investment Opportunity.
- Huisman, J., Pham Thi, N. N., Karl, D. M., & Sommeijer, B. (2006). Reduced mixing generates oscillations and chaos in the oceanic deep chlorophyll maximum. *Nature*, *439*(7074), 322–325. <https://doi.org/10.1038/nature04245>
- Kallen, R., Morse, K., Grosse, D., & Leonard, D. (2001). Small-Scale Oyster Farming for Chesapeake Watermen: A Sustainable Business Marketing Plan. *Washington, DC: TerraAqua Environmental Science and Policy, LLC. Prepared for the Campbell Foundation for the Environment.*
- Karlson, B., Cusack, C., & Bresnan, E. (Eds.). (2010). Microscopic and Molecular Methods for Quantitative Phytoplankton Analysis. *Intergovernmental Oceanographic Commission*, 55.
- Kolb, A., Hannach, G., & Swanson, L. (2016). Marine Phytoplankton Monitoring Program Sampling and Analysis Plan. *King County Department of Natural Resources and Parks Water and Land Resources Division.*
- Kuha, J., Järvinen, M., Salmi, P., & Karjalainen, J. (2019). Calibration of in situ chlorophyll fluorometers for organic matter. *Hydrobiologia*, *847*(21), 4377–4387. <https://doi.org/10.1007/s10750-019-04086-z>
- Lee, M., Won, N.-I., & Baek, S. H. (2020). Comparison of HPLC Pigment Analysis and Microscopy in Phytoplankton Assessment in the Seomjin River Estuary, Korea. *Sustainability*, *12*(4). <https://doi.org/10.3390/su12041675>
- Marine Aquaculture Task Force. (2007). (rep.). *Sustainable Marine Aquaculture: Fulfilling The Promise; Managing The Risks*. Takoma Park, Maryland.
- Martin, A. P. (2003). Phytoplankton patchiness: the role of lateral stirring and mixing. *Progress in Oceanography*, *57*(2), 125–174. [https://doi.org/10.1016/s0079-6611\(03\)00085-5](https://doi.org/10.1016/s0079-6611(03)00085-5)
- Matthews, K. (2019, August 30). *How big data analytics are impacting the agriculture industry*. VXCHANGE. <https://www.vxchnge.com/blog/data-centers-analytics-and-agriculture>.
- Milne, B. F., Toker, Y., Rubio, A., & Nielsen, S. B. (2015). Unraveling the Intrinsic Color of Chlorophyll. *Angewandte Chemie International Edition*, *54*(7), 2170–2173. <https://doi.org/10.1002/anie.201410899>

- Mishra, S., & Mishra, D. R. (2012). Normalized difference chlorophyll index: A novel model for remote estimation of chlorophyll-a concentration in turbid productive waters. *Remote Sensing of Environment*, 117, 394-406.
- Nam, H., An, S., Kim, C.-H., Park, S.-H., Kim, Y.-W., & Lim, S.-H. (2015). Remote monitoring system based on ocean sensor networks for offshore aquaculture. *Oceans*. <https://doi.org/10.1109/oceans.2014.7003046>
- National Center for Biotechnology Information (2021). PubChem Compound Summary for CID 12085802, Chlorophyll a. Retrieved June 29, 2021
- National Oceanic and Atmospheric Administration (NOAA). (2019, April 2). What is aquaculture?. Retrieved from <https://www.fisheries.noaa.gov/topic/aquaculture#>
- National Oceanic and Atmospheric Administration (NOAA). (2020, April 17). U.S. Aquaculture. National Oceanic and Atmospheric Administration (NOAA). (2021). *How much oxygen comes from the ocean?* NOAA's National Ocean Service.
- National Sea Grant Law Center. (2019, November 5). *Shellfish Aquaculture - The Basics*. Law on the Half Shell. <https://nsglc.olemiss.edu/lawonthehalfshell/files/ep1-shownotes.pdf>.
- National Weather Service. (2021). *National Weather Service Weather Archives - Data and Maps*. National Weather Service Forecast Office. <https://w2.weather.gov/climate/index.php?wfo=ffc>.
- NCSitingTool. (2021) NC Shellfish Lease Siting Tool (UNCW) [map]. Layers used: Bottom Type, Salinity, Shellfish Leases 2020. Rudolf, M.; using "The North Carolina Shellfish Siting Tool" (Accessed August 1, 2021
- N.C. Division of Marine Fisheries. (2021). *NC Shellfish Lease and Aquaculture Permitting Program*. North Carolina Environmental Quality. <http://portal.ncdenr.org/web/mf/shellfish-lease-franchise-programs>.
- Nell, J. A. (2002). Farming triploid oysters. *Aquaculture*, 210(1-4), 69-88.
- Ore, J.P., Elbaum, S., Burgin, A., Zhao, B., & Detweiler, C. (2015). Autonomous Aerial Water Sampling. *Springer Tracts in Advanced Robotics, Field and Service Robotics*, 137–151. [https://doi.org/10.1007/978-3-319-07488-7\\_10](https://doi.org/10.1007/978-3-319-07488-7_10)
- Powell, E. N., Klinck, J. M., Hofmann, E. E., Wilson-Ormond, E. A., & Ellis, M. S. (1995). Modeling oyster populations. V. Declining phytoplankton stocks and the population dynamics of American oyster (*Crassostrea virginica*) populations. *Fisheries Research*, 24(3), 199-222.
- Proagrica. (2021). *How data analytics is transforming agriculture*. Proagrica. <https://proagrica.com/news/how-data-analytics-is-transforming-agriculture/>.

- PwC Norway. (2021). *Seafood Barometer 2021*.  
<https://www.pwc.no/en/publications/seafood-barometer.html>.
- Rice, E. W., Baird, R. B., & Eaton, A. D. (Eds.). (2018). *10200 PLANKTON*. Standard Methods for the Examination of Water and Wastewater.
- Shen, L., Xu, H., & Guo, X. (2012). Satellite Remote Sensing of Harmful Algal Blooms (HABs) and a Potential Synthesized Framework. *Sensors*, *12*(6), 7778–7803.  
<https://doi.org/10.3390/s120607778>
- Small Unmanned Aircraft Systems, 14 C.F.C § 107 (2021)
- Smith, D., Cross, L., Rivet, J., & Hall, S. (2015). Design of a semi-autonomous boat for measurements of coastal sedimentation and erosion. *Proceedings of the International Association of Hydrological Sciences*, *367*, 447.
- Souza, M. (2019, August 22). 5 Problems Inherent to Aquaculture.
- Taylor, A., Tykol, A., Silvia, C., Smith, D. D., Cotlar, S., & Hall, S. G. (2014). Development of an Autonomous Boat for Sustainable Aquatic Plant Biomass Collection. In *2014 Montreal, Quebec Canada July 13–July 16, 2014* (p. 1). American Society of Agricultural and Biological Engineers.
- The Fish Site. (2020, April 27). Challenges Facing Aquaculture.
- Tweddle, J. F., Gubbins, M., & Scott, B. E. (2018). Should phytoplankton be a key consideration for marine management? *Marine Policy*, *97*, 1–9.  
<https://doi.org/10.1016/j.marpol.2018.08.026>
- United States Geological Survey. (2021). EarthExplorer. <https://earthexplorer.usgs.gov/>.
- United States Geological Survey. (2020). *Landsat Level-1 Processing Details*. Landsat Mission. <https://www.usgs.gov/core-science-systems/nli/landsat/landsat-level-1-processing-details>.
- United States Geological Survey. (2020). Landsat Missions. Retrieved November 16, 2020.
- Villareal, T. A., Adornato, L., Wilson, C., & Schoenbaechler, C. A. (2011). Summer blooms of diatom-diazotroph assemblages and surface chlorophyll in the North Pacific gyre: A disconnect. *Journal of Geophysical Research*, *116*(C3).  
<https://doi.org/10.1029/2010jc006268>
- Von Tress, N., Nelson, N., & Young, S. (2021, May 27). *Supporting Cyanobacterial Bloom Monitoring with Satellite Imagery*. NC State Extension Publications.  
<https://content.ces.ncsu.edu/supporting-cyanobacterial-bloom-monitoring-with-satellite-imagery>.
- Wagner, A. (2018, May 30). Could N.C. become the 'Napa Valley of oysters?'.

- Watanabe, F. S. Y., Alcântara, E., Rodrigues, T. W. P., Imai, N. N., Barbosa, C. C. F., & Rotta, L. H. D. S. (2015). Estimation of chlorophyll-a concentration and the trophic state of the Barra Bonita hydroelectric reservoir using OLI/Landsat-8 images. *International journal of environmental research and public health*, 12(9), 10391-10417.
- Weissberger, E. J., & Glibert, P. M. (2021). Diet of the eastern oyster, *Crassostrea virginica*, growing in a eutrophic tributary of Chesapeake Bay, Maryland, USA. *Aquaculture Reports*, 20. <https://doi.org/10.1016/j.aqrep.2021.100655>
- White, C. (2018, July 20). Technical report: Global aquaculture market's growth accelerating through 2022.
- White, K., O'Neill, B., & Tzankova, Z. (2004). At a crossroads: will aquaculture fulfill the promise of the blue revolution. *Silver Spring Meriland SeaWeb*: [http://www.seaweb.org/resources/documents/reports\\_crossroads.pdf](http://www.seaweb.org/resources/documents/reports_crossroads.pdf).
- Wilson, C. (2003). Late Summer chlorophyll blooms in the oligotrophic North Pacific Subtropical Gyre. *Geophysical Research Letters*, 30(18). <https://doi.org/10.1029/2003gl017770>
- Wilson, C., & Qiu, X. (2008). Global distribution of summer chlorophyll blooms in the oligotrophic gyres. *Progress in Oceanography*, 78(2), 107–134. <https://doi.org/10.1016/j.pocean.2008.05.002>
- Wilson, C., Villareal, T. A., Maximenko, N., Bograd, S. J., Montoya, J. P., & Schoenbaechler, C.A. (2008). Biological and physical forcings of late summer chlorophyll blooms at 30°N in the oligotrophic Pacific. *Journal of Marine Systems*, 69(3-4), 164–176. <https://doi.org/10.1016/j.jmarsys.2005.09.018>
- Zeng, L., & Li, D. (2015). Development of In Situ Sensors for Chlorophyll Concentration Measurement. *Journal of Sensors*, 2015. <https://doi.org/10.1155/2015/903509>

# APPENDICES

## Appendix A

<b>Ground Control Points</b>							
<b>Site</b>	<b>Date</b>	<b>Right GCP</b>		<b>Left GCP</b>		<b>Back GCP</b>	
		<b>Latitude</b>	<b>Longitude</b>	<b>Latitude</b>	<b>Longitude</b>	<b>Latitude</b>	<b>Longitude</b>
Ward Creek	10/12/2020	34.77095	-76.59053	34.77076	-76.59010	34.77106	-76.59039
Ward Creek	11/11/2020	34.77098	-76.59050	34.77080	-76.59010	34.77103	-76.59025

<b>Sampling Locations</b>				
	<b>10/12/2020</b>		<b>11/11/2020</b>	
<b>Point</b>	<b>Latitude</b>	<b>Longitude</b>	<b>Latitude</b>	<b>Longitude</b>
A	34.77027	-76.59073	34.77016	-76.59071
B	34.76987	-76.59013	34.76973	-76.58965
C	34.76928	-76.58871	34.76936	-76.58876
D	34.76883	-76.58898	34.76890	-76.58930
E	34.76921	-76.58993	34.76936	-76.59045
F	34.76946	-76.59045	34.76981	-76.59065

<b>Ward Creek UAV Image Camera Locations (10/12/2020)</b>		
<b>Image</b>	<b>Latitude</b>	<b>Longitude</b>
DJI_0001	34.76925	-76.59
DJI_0002	34.76926	-76.5897
DJI_0003	34.76926	-76.5894
DJI_0004	34.76926	-76.5892
DJI_0005	34.76926	-76.5889
DJI_0006	34.76958	-76.5889
DJI_0007	34.76957	-76.5892
DJI_0008	34.76957	-76.5894
DJI_0009	34.76957	-76.5897
DJI_0010	34.76957	-76.59
DJI_0011	34.76957	-76.5903
DJI_0012	34.76957	-76.5906
DJI_0013	34.76957	-76.5909
DJI_0014	34.76957	-76.5909
DJI_0015	34.76989	-76.5908
DJI_0016	34.76988	-76.5906
DJI_0017	34.76988	-76.5903
DJI_0018	34.76988	-76.59
DJI_0019	34.76988	-76.5897

<b>Ward Creek UAV Image Camera Locations (10/12/2020)</b> (continued)		
<b>Image</b>	<b>Latitude</b>	<b>Longitude</b>
DJI_0020	34.76988	-76.5894
DJI_0021	34.76988	-76.5892
DJI_0022	34.76988	-76.5889
DJI_0023	34.76988	-76.5888
DJI_0024	34.7702	-76.5887
DJI_0025	34.77019	-76.589
DJI_0026	34.77019	-76.5893
DJI_0027	34.77019	-76.5896
DJI_0028	34.77019	-76.5899
DJI_0029	34.77019	-76.5902
DJI_0030	34.77019	-76.5904
DJI_0031	34.77019	-76.5907
DJI_0032	34.77019	-76.5908
DJI_0033	34.77052	-76.5907
DJI_0034	34.7705	-76.5904
DJI_0035	34.7705	-76.5901
DJI_0036	34.7705	-76.5898
DJI_0037	34.7705	-76.5896
DJI_0038	34.7705	-76.5893
DJI_0039	34.7705	-76.5892
DJI_0040	34.77082	-76.5901
DJI_0041	34.77081	-76.5903
DJI_0042	34.77081	-76.5906
DJI_0043	34.77081	-76.5906

<b>Ward Creek UAV Image Camera Locations (11/11/2020)</b>		
<b>Image</b>	<b>Latitude</b>	<b>Longitude</b>
DJI_0104	34.76983	-76.5889
DJI_0105	34.76982	-76.5892
DJI_0106	34.76983	-76.5896
DJI_0107	34.76982	-76.5899
DJI_0108	34.76982	-76.59
DJI_0109	34.77017	-76.5907
DJI_0110	34.77016	-76.5904
DJI_0111	34.77016	-76.59
DJI_0112	34.77017	-76.5897
DJI_0113	34.77017	-76.5894

<b>Ward Creek UAV Image Camera Locations (11/11/2020)</b> (continued)		
<b>Image</b>	<b>Latitude</b>	<b>Longitude</b>
DJI_0114	34.77016	-76.5891
DJI_0115	34.77016	-76.5888
DJI_0116	34.77017	-76.5888
DJI_0117	34.77052	-76.5892
DJI_0118	34.77052	-76.5895
DJI_0119	34.77051	-76.5899
DJI_0120	34.77052	-76.5902
DJI_0121	34.77052	-76.5905
DJI_0122	34.77053	-76.5905
DJI_0123	34.77088	-76.5903
DJI_0124	34.77086	-76.5901

## Appendix B

<b>Chlorophyll-a Concentrations</b>										
Site	Date	Sample	Volume filtered (L)	Volume of extractant (mL)	Wavelength (µm)					Pheophytin-corrected chlorophyll (µg/L)
					630	647	664	665	750	
Ward Creek	10/12/2020	A	0.510	10	0.007	0.009	0.027	0.026	0.001	0.523529
		B	0.510	10	0.007	0.009	0.032	0.031	0.000	0.523529
		C	0.509	10	0.008	0.01	0.031	0.03	0.002	0.524558
		D	0.507	11	0.007	0.009	0.026	0.025	0.001	0.579290
		E	0.511	10	0.025	0.027	0.047	0.046	0.016	0.522505
Ward Creek	11/11/2020	A	0.537	10	-0.001	0.000	0.023	0.022	-0.013	0.497207
		B	0.535	10	-0.002	-0.001	0.018	0.017	-0.013	0.499065
		C	0.518	10	0.002	0.003	0.022	0.021	-0.009	0.515444
		D	0.527	10	-0.002	0.000	0.021	0.02	-0.013	0.506641
		E	0.523	10	-0.004	-0.002	0.019	0.018	-0.014	0.510516
		F	0.523	10	-0.005	-0.002	0.02	0.019	-0.017	0.510516

## Appendix C

Indexed Point Values						
Date	Image	Point	buffer (ft)	ExG	nRAVI	RAVI
10/12/2020	16	A	9	6.682643	.001649	1.003344
10/12/2020	16	B	9	-.113543	.015063	1.030707
10/12/2020	16	F	9	2.370201	.014654	1.029895
10/12/2020	17	A	9	5.395397	.002241	1.004524
10/12/2020	17	B	9	3.665235	.020961	1.042965
10/12/2020	17	F	9	5.422739	.020989	1.043002
10/12/2020	18	B	9	9.618364	.027070	1.055791
10/12/2020	18	F	9	5.485485	.030512	1.063120
10/12/2020	19	B	9	6.241327	.029314	1.060589
10/12/2020	19	E	9	-.314496	.025615	1.052719
10/12/2020	27	B	9	1.059113	.040252	1.084031
10/12/2020	28	B	9	3.925971	.022143	1.045455
10/12/2020	29	A	9	4.146752	.023293	1.047797
10/12/2020	29	B	9	2.749318	.015614	1.031873
10/12/2020	30	A	9	7.410019	.022559	1.046251
10/12/2020	31	A	9	8.187381	.015745	1.032107
10/12/2020	32	A	9	8.352090	.014436	1.029405
10/12/2020	33	A	9	10.180164	.026099	1.053726
10/12/2020	34	A	9	8.609688	.043541	1.091194
10/12/2020	34	B	9	.047434	.019038	1.038899
10/12/2020	35	B	9	6.031509	.025927	1.053369
10/12/2020	36	B	9	8.293210	.040117	1.083672
10/12/2020	40	A	9	3.572655	.053402	1.113000
10/12/2020	41	A	9	4.269807	.033725	1.069925
10/12/2020	42	A	9	5.676738	.028975	1.059809
10/12/2020	43	A	9	5.933298	.049012	1.067902

Indexed Point Values (continued)						
11/11/2020	104	C	9	8.661794	.043776	1.091735
11/11/2020	104	D	9	14.559152	.062583	1.133685
11/11/2020	105	B	9	12.829983	.049121	1.103445
11/11/2020	106	B	9	13.905912	.039770	1.082950
11/11/2020	107	B	9	9.056238	.022817	1.046803
11/11/2020	108	B	9	6.518859	.018909	1.038667
11/11/2020	108	E	9	14.484459	.037076	1.077165
11/11/2020	109	A	9	12.531643	.032413	1.067162
11/11/2020	109	F	9	14.548163	.039226	1.081777
11/11/2020	110	A	9	10.817992	.035097	1.072900
11/11/2020	110	F	9	17.394637	.047202	1.099177
11/11/2020	111	B	9	4.779591	.033476	1.069505
11/11/2020	112	B	9	10.928648	.052389	1.110770
11/11/2020	113	B	9	12.664165	.064835	1.138955
11/11/2020	114	B	9	14.576752	.077898	1.169264
11/11/2020	120	A	9	14.527020	.062870	1.134371
11/11/2020	120	F	9	14.363675	.068665	1.147664
11/11/2020	121	A	9	16.308327	.059739	1.127219
11/11/2020	121	F	9	13.580632	.057954	1.123219
11/11/2020	122	A	9	16.355855	.059150	1.125908
11/11/2020	122	F	9	14.417483	.059485	1.126688
11/11/2020	123	A	9	13.998379	.074546	1.161367
10/12/2020	16	A	20	6.701760	.002074	1.004203
10/12/2020	16	B	20	.070603	.014135	1.028810
10/12/2020	16	F	20	2.128809	.015875	1.032404
10/12/2020	17	A	20	5.170862	.002996	1.006050
10/12/2020	17	B	20	4.453159	.020924	1.042892
10/12/2020	17	F	20	5.094548	.020002	1.040982
10/12/2020	18	B	20	9.910115	.025468	1.052413
10/12/2020	18	F	20	5.189478	.030002	1.062072

Indexed Point Values (continued)						
10/12/2020	19	B	20	6.945147	.028863	1.059611
10/12/2020	19	E	20	-.801690	.024956	1.051356
10/12/2020	20	E	20	1.193028	.039594	1.082584
10/12/2020	27	B	20	1.174859	.038542	1.080320
10/12/2020	28	B	20	3.873004	.021133	1.043334
10/12/2020	29	A	20	4.265087	.024117	1.049559
10/12/2020	29	B	20	2.893321	.015284	1.031175
10/12/2020	30	A	20	7.155544	.021440	1.043941
10/12/2020	31	A	20	8.352509	.015193	1.030980
10/12/2020	32	A	20	8.313088	.014293	1.029125
10/12/2020	33	A	20	10.639019	.027041	1.055736
10/12/2020	34	A	20	8.441058	.043992	1.092267
10/12/2020	34	B	20	-.256551	.017390	1.035472
10/12/2020	35	B	20	6.264104	.026806	1.055230
10/12/2020	36	B	20	7.916534	.039772	1.082954
10/12/2020	40	A	20	3.887811	.055032	1.116684
10/12/2020	41	A	20	4.501889	.033541	1.069552
10/12/2020	42	A	20	6.028273	.030787	1.063663
10/12/2020	43	A	20	6.497862	.032762	1.067874
11/11/2020	104	C	20	8.930708	.044245	1.092765
11/11/2020	104	D	20	14.581578	.062865	1.134367
11/11/2020	105	B	20	13.180609	.048353	1.101765
11/11/2020	106	B	20	13.064392	.039435	1.082273
11/11/2020	107	B	20	8.710267	.023879	1.049059
11/11/2020	108	B	20	6.290821	.017184	1.035098
11/11/2020	108	E	20	14.377747	.039458	1.082299
11/11/2020	108	F	20	8.554496	.034259	1.071098
11/11/2020	109	A	20	12.476306	.031441	1.065096
11/11/2020	109	F	20	14.077009	.038848	1.080980
11/11/2020	110	A	20	10.836704	.036773	1.076504

Indexed Point Values (continued)						
11/11/2020	110	F	20	16.851130	.046214	1.097036
11/11/2020	111	B	20	5.861850	.033988	1.070597
11/11/2020	112	B	20	11.772338	.052723	1.111492
11/11/2020	113	B	20	14.169244	.066685	1.143163
11/11/2020	114	B	20	14.529072	.078103	1.169746
11/11/2020	120	A	20	14.712708	.063321	1.135396
11/11/2020	120	F	20	15.241657	.069777	1.150285
11/11/2020	121	A	20	16.361653	.059224	1.126078
11/11/2020	121	F	20	14.430201	.060257	1.128488
11/11/2020	122	A	20	15.969170	.076706	1.123771
11/11/2020	122	F	20	13.915857	.070291	1.125521
11/11/2020	123	A	20	14.198590	.076520	1.166014
11/11/2020	124	A	20	16.961538	.085669	1.187725
10/12/2020	16	A	50	6.919578	.002866	1.005801
10/12/2020	16	B	50	.079390	.012880	1.026243
10/12/2020	16	F	50	1.409069	.014826	1.030238
10/12/2020	17	A	50	4.725758	.004766	1.009638
10/12/2020	17	B	50	4.467480	.019215	1.039326
10/12/2020	17	F	50	5.149287	.020279	1.041550
10/12/2020	18	B	50	8.846655	.024932	1.051295
10/12/2020	18	F	50	5.598980	.029852	1.061743
10/12/2020	19	B	50	7.274988	.028962	1.059828
10/12/2020	19	E	50	-.135646	.025695	1.052969
10/12/2020	20	E	50	1.348406	.037857	1.078855
10/12/2020	26	B	50	3.445214	.031866	1.065963
10/12/2020	27	B	50	1.023422	.034357	1.071307
10/12/2020	28	A	50	.477748	.029585	1.061054
10/12/2020	28	B	50	4.035384	.020206	1.041372
10/12/2020	29	A	50	4.121682	.026626	1.054941
10/12/2020	29	B	50	3.136478	.013827	1.028165

Indexed Point Values (continued)						
10/12/2020	30	A	50	7.619348	.020429	1.041878
10/12/2020	31	A	50	8.195442	.014088	1.028698
10/12/2020	32	A	50	8.028128	.013311	1.027113
10/12/2020	33	A	50	10.019178	.029067	1.060050
10/12/2020	34	A	50	8.061014	.042009	1.087960
10/12/2020	34	B	50	1.244083	.018473	1.037721
10/12/2020	35	A	50	4.737437	.047780	1.100505
10/12/2020	35	B	50	5.593886	.028202	1.058189
10/12/2020	36	B	50	7.843393	.041085	1.085850
10/12/2020	37	B	50	6.976148	.043253	1.090530
10/12/2020	40	A	50	3.778334	.052946	1.112150
10/12/2020	41	A	50	5.069801	.034511	1.071647
10/12/2020	42	A	50	5.918737	.030043	1.062104
10/12/2020	43	A	50	6.215488	.031457	1.065112
11/11/2020	104	B	50	9.308445	.051165	1.108006
11/11/2020	104	C	50	9.339398	.045224	1.094933
11/11/2020	104	D	50	15.114040	.063180	1.135123
11/11/2020	105	B	50	12.956941	.047629	1.100167
11/11/2020	106	B	50	12.685378	.038434	1.080103
11/11/2020	107	B	50	8.771200	.023941	1.049192
11/11/2020	107	E	50	14.275899	.044981	1.094308
11/11/2020	108	A	50	1.587287	.030518	1.063142
11/11/2020	108	B	50	5.946276	.016860	1.034432
11/11/2020	108	E	50	13.714680	.039288	1.081940
11/11/2020	108	F	50	8.914470	.034483	1.071578
11/11/2020	109	A	50	12.399604	.031939	1.066165
11/11/2020	109	E	50	5.193132	.030194	1.062472
11/11/2020	109	F	50	13.707887	.038465	1.080182
11/11/2020	110	A	50	11.374803	.038402	1.080029
11/11/2020	110	E	50	10.913203	.042260	1.088442

Indexed Point Values (continued)						
11/11/2020	110	F	50	16.313390	.046892	1.098535
11/11/2020	111	A	50	10.975143	.048882	1.102914
11/11/2020	111	B	50	5.402297	.033400	1.069327
11/11/2020	111	E	50	14.664648	.060830	1.129790
11/11/2020	111	F	50	14.725173	.054254	1.114886
11/11/2020	112	B	50	11.425256	.051968	1.109824
11/11/2020	113	B	50	14.076738	.066592	1.142944
11/11/2020	114	B	50	14.764233	.077641	1.168656
11/11/2020	117	B	50	20.539955	.079656	1.173187
11/11/2020	118	B	50	13.906456	.065647	1.140719
11/11/2020	119	B	50	8.516390	.059512	1.126843
11/11/2020	120	A	50	15.116055	.063363	1.135499
11/11/2020	120	F	50	15.240064	.068010	1.146252
11/11/2020	121	A	50	16.105977	.058696	1.124903
11/11/2020	121	F	50	14.354073	.059521	1.126795
11/11/2020	122	A	50	15.535221	.057485	1.122174
11/11/2020	122	F	50	13.797372	.058427	1.124312
11/11/2020	123	A	50	15.042655	.077714	1.168831
11/11/2020	124	A	50	16.536883	.082884	1.181058

## Appendix D

Removed Images							
Dataset	Image	Point	Buffer size	True chl-a	ExG	nRAVI	RAVI
10/12/2020	33	B	50	0.523529	-2.01191	0.016413	1.033436
10/12/2020	32	F	9	0.518447	-6.12798	0.003581	1.007265
10/12/2020	32	F	20	0.518447	-6.30456	0.003885	1.007881
10/12/2020	32	F	50	0.518447	-5.50367	0.001362	1.002807
10/12/2020	31	B	50	0.523529	2.348553	0.0017	1.003498
10/12/2020	31	F	9	0.518447	-2.85449	0.008344	1.016903
10/12/2020	31	F	20	0.518447	-2.94892	0.005939	1.012034
10/12/2020	31	F	50	0.518447	-3.0034	0.003589	1.007282
10/12/2020	30	B	9	0.523529	-3.23775	0.004847	1.009814
10/12/2020	30	B	20	0.523529	-2.77056	0.00558	1.011305
10/12/2020	30	B	50	0.523529	-2.00273	0.006039	1.012233
10/12/2020	30	F	50	0.518447	-1.51755	0.008504	1.017256
10/12/2020	29	F	50	0.518447	-3.93193	0.016049	1.032737
10/12/2020	28	F	20	0.518447	-3.20894	0.043355	1.090799
10/12/2020	28	F	50	0.518447	-2.3333	0.035776	1.074379
10/12/2020	27	F	50	0.518447	-4.23329	0.060819	1.12967
10/12/2020	22	C	50	0.524558	-2.4113	0.020578	1.042106
10/12/2020	23	C	50	0.524558	-2.70161	0.022264	1.045632
10/12/2020	18	E	9	0.522505	-5.85149	0.008117	1.016459
10/12/2020	18	E	20	0.522505	-5.67746	0.009319	1.018919
10/12/2020	18	E	50	0.522505	-3.93367	0.012828	1.026143
10/12/2020	17	E	9	0.522505	-10.7483	0.004431	1.00898
10/12/2020	17	E	20	0.522505	-10.3378	0.005889	1.011924
10/12/2020	17	E	50	0.522505	-8.44405	0.006567	1.013307
10/12/2020	14	A	50	0.523529	7.251671	0.000784	1.001616
10/12/2020	13	A	50	0.523529	6.382626	0.001712	1.003474

Removed Images (continued)							
10/12/2020	16	E	50	0.522505	-12.6211	0.001882	1.003927
10/12/2020	16	E	20	0.522505	-21.4286	0.008732	1.017636
10/12/2020	20	C	50	0.524558	-16.6688	-0.00445	0.991147
10/12/2020	20	C	20	0.524558	-18.5	-0.00594	0.988189
10/12/2020	20	C	9	0.524558	0.780943	0.040571	1.084712
10/12/2020	32	B	50	0.523529	0.820513	-0.00792	0.984355
11/11/2020	105	C	9	0.515444	-0.69235	0.02295	1.04718
11/11/2020	105	C	20	0.515444	-0.61043	0.023132	1.047586
11/11/2020	105	C	50	0.515444	-0.30063	0.024065	1.04957
11/11/2020	106	C	9	0.515444	-18.4355	-0.00095	0.981162
11/11/2020	106	C	20	0.515444	-18.141	-0.00795	0.984513
11/11/2020	106	C	50	0.515444	-12.2639	0.000408	1.001151
11/11/2020	110	B	9	0.499065	-6.05757	0.007797	1.016295
11/11/2020	110	B	20	0.499065	-4.3619	0.011754	1.023976
11/11/2020	110	B	50	0.499065	-4.12703	0.012101	1.024742
11/11/2020	120	B	20	0.499065	-1.11098	0.041968	1.087759
11/11/2020	120	B	50	0.499065	-0.2529	0.040263	1.084263
11/11/2020	121	B	50	0.499065	-14.6115	0.008303	1.017376
11/11/2020	122	B	50	0.499065	-16.403	0.004863	0.101017
10/12/2020	13	F	9	0.518447	-3.78011	-0.00126	0.997539
10/12/2020	13	F	20	0.518447	-3.33102	0.000193	1.000453
10/12/2020	13	F	50	0.518447	-2.0127	0.000931	1.00192
10/12/2020	14	F	9	0.518447	-6.3473	-0.00284	0.994385
10/12/2020	14	F	20	0.518447	-5.98635	-0.00226	0.995562
10/12/2020	14	F	50	0.518447	-4.55335	-0.00121	0.997635
10/12/2020	15	A	9	0.523529	8.724527	0.001833	1.003711
10/12/2020	15	A	20	0.523529	8.180853	0.002463	1.004983
10/12/2020	15	A	50	0.523529	7.527348	0.003578	1.007936
10/12/2020	15	B	9	0.523529	-7.2861	0.008206	1.016639
10/12/2020	15	B	20	0.523529	-7.13928	0.009046	1.018374

<b>Removed Images (continued)</b>							
10/12/2020	15	B	50	0.523529	-6.19337	0.007582	1.016129
10/12/2020	15	F	9	0.518447	-8.3388	0.00729	1.014787
10/12/2020	15	F	20	0.518447	-8.07349	0.007514	1.015249
10/12/2020	15	F	50	0.518447	-7.09523	0.007988	1.016129

## Appendix E

<b>Linear/Multilinear Regression Models</b>				
<b>Index+Buffer</b>	<b>Intercept</b>	<b>ExG</b>	<b>nRAVI</b>	<b>RAVI</b>
ExG+nRAVI+RAVI (9ft)	0.773768	-0.001140	0.385388	-0.245630
nRAVI+RAVI (9ft)	0.930449	0	0.524148	-0.405070
ExG+RAVI (9ft)	0.596081	-0.001162	0	-0.067230
ExG+nRAVI (9ft)	0.528885	-0.001213	-0.128870	0
RAVI (9ft)	0.691253	0	0	-0.164980
nRAVI (9ft)	0.526353	0	-0.345550	0
ExG (9ft)	0.527073	-0.001551	0	0
RAVI (20ft)	0.685116	0	0	-0.159120
nRAVI (20ft)	0.526208	0	-0.335330	0
ExG+RAVI (20ft)	0.587552	-0.001199	0	-0.058950
ExG+nRAVI+RAVI (20ft)	0.566500	-0.001193	-0.045700	-0.037880
ExG+nRAVI (20ft)	0.528625	-0.001194	-0.124170	0
nRAVI+RAVI (20ft)	0.567905	0	-0.248860	-0.041700
ExG (20ft)	0.527127	-0.001562	0	0
RAVI (50ft)	0.689760	0	0	-0.163620
ExG+nRAVI+RAVI (50ft)	0.409789	-0.000949	-0.426680	0.118142
ExG+RAVI (50ft)	0.604701	-0.000944	0	-0.077400
nRAVI+RAVI (50ft)	0.841278	0	0.332558	-0.315620
nRAVI (50ft)	0.526647	0	-0.357610	0
ExG+nRAVI (50ft)	0.527555	-0.000945	-0.169190	0
ExG (50ft)	0.525031	-0.001417	0	0

<b>Linear/Multilinear Regression Models and R<sup>2</sup></b>					
<b>Index</b>	<b>Multiple R</b>	<b>R<sup>2</sup></b>	<b>Adjusted R<sup>2</sup></b>	<b>Standard Error</b>	<b>Observations</b>
ExG+RAVI (20ft)	0.730	0.533	0.513	0.008	51
ExG+nRAVI (20ft)	0.730	0.532	0.513	0.008	51
ExG+nRAVI+RAVI (20ft)	0.730	0.533	0.503	0.008	51
ExG (20ft)	0.712	0.507	0.497	0.008	51
ExG+RAVI (9ft)	0.713	0.509	0.487	0.008	48
ExG+nRAVI+RAVI (9ft)	0.718	0.516	0.483	0.008	48
ExG+nRAVI (9ft)	0.709	0.503	0.481	0.008	48
ExG (9ft)	0.691	0.477	0.466	0.008	48
ExG+nRAVI (50ft)	0.683	0.466	0.45	0.008	66
ExG+RAVI (50ft)	0.683	0.466	0.449	0.008	66
ExG+nRAVI+RAVI (50ft)	0.683	0.467	0.441	0.008	66
ExG (50ft)	0.655	0.429	0.42	0.008	66
nRAVI (20ft)	0.626	0.392	0.379	0.009	51
RAVI (50ft)	0.618	0.382	0.373	0.009	66
nRAVI (50ft)	0.618	0.382	0.372	0.009	66
RAVI (20ft)	0.623	0.388	0.375	0.009	51
nRAVI+RAVI (50ft)	0.618	0.382	0.363	0.009	66
nRAVI+RAVI (20ft)	0.626	0.392	0.367	0.009	51
RAVI (9ft)	0.609	0.371	0.358	0.009	48
nRAVI+RAVI (9ft)	0.620	0.385	0.357	0.009	48
nRAVI (9ft)	0.589	0.347	0.333	0.009	48

<b>RMSE</b>	
<b>Index</b>	<b>RMSE</b>
ExG+nRAVI+RAVI (20ft)	0.00733850
ExG+RAVI (20ft)	0.00747319
ExG+nRAVI (20ft)	0.00756457
ExG+nRAVI+RAVI (9ft)	0.00762237
ExG+RAVI (9ft)	0.00765699
ExG (20ft)	0.00766373
RAVI (9ft)	0.00769799
ExG (9ft)	0.00769096
ExG+nRAVI+RAVI (50ft)	0.00793237
ExG+nRAVI (50ft)	0.00801317
ExG+RAVI (50ft)	0.00795729
ExG (50ft)	0.00821261
nRAVI+RAVI (20ft)	0.00851664
nRAVI (20ft)	0.00851944
RAVI (20ft)	0.00858121
nRAVI+RAVI (50ft)	0.00853560
RAVI (50ft)	0.00856061
nRAVI (50ft)	0.00856369
nRAVI+RAVI (9ft)	0.00841040
ExG+nRAVI (9ft)	0.00862381
nRAVI (9ft)	0.00881926

Actual and Predicted Chl-a Concentrations by Model											
Date	Image	Point	Buffer (ft)	Actual Chl-a	Predicted Chl-a by Model						
					ExG	nRAVI	RAVI	ExG+nRAVI	ExG+RAVI	nRAVI+RAVI	ExG+nRAVI+RAVI
10/12/2020	16	A	9	.523529	.516711	.525783	.525723	.520565	.520859	.524889	.520339
10/12/2020	16	B	9	.523529	.527250	.521148	.521208	.527081	.526916	.520836	.526534
10/12/2020	16	F	9	.518447	.523398	.521289	.521342	.524121	.524085	.520951	.523744
10/12/2020	17	A	9	.523529	.518707	.525578	.525528	.522051	.522275	.524722	.521745
10/12/2020	17	B	9	.523529	.521390	.519110	.519186	.521737	.521701	.518962	.521489
10/12/2020	17	F	9	.518447	.518664	.519100	.519180	.519601	.519657	.518962	.519487
10/12/2020	18	B	9	.523529	.512158	.516999	.517070	.513728	.513922	.516969	.513908
10/12/2020	18	F	9	.518447	.518567	.515809	.515861	.518298	.518231	.515804	.518144
10/12/2020	19	B	9	.523529	.517395	.516223	.516278	.517535	.517523	.516202	.517443
10/12/2020	19	E	9	.522505	.527561	.517501	.517577	.525965	.525669	.517451	.525422
10/12/2020	27	B	9	.523529	.525431	.512444	.512411	.522413	.521968	.512439	.521807
10/12/2020	28	B	9	.523529	.520985	.518701	.518775	.521268	.521231	.518573	.521036
10/12/2020	29	A	9	.523529	.520643	.518304	.518389	.520852	.520817	.518227	.520652
10/12/2020	29	B	9	.523529	.522810	.520957	.521016	.523537	.523511	.520653	.523197
10/12/2020	30	A	9	.523529	.515583	.518557	.518644	.516988	.517129	.518469	.517029
10/12/2020	31	A	9	.523529	.514377	.520912	.520977	.516923	.517177	.520627	.516992
10/12/2020	32	A	9	.523529	.514122	.521364	.521423	.516892	.517167	.521035	.516963
10/12/2020	33	A	9	.523529	.511287	.517334	.517411	.513171	.513408	.517296	.513400
10/12/2020	34	A	9	.523529	.513722	.511307	.511229	.512829	.512714	.511261	.512709
10/12/2020	34	B	9	.523529	.527000	.519774	.519857	.526374	.526178	.519601	.525870
10/12/2020	35	B	9	.523529	.517720	.517394	.517469	.518227	.518252	.517351	.518150
10/12/2020	36	B	9	.523529	.514213	.512490	.512470	.513654	.513587	.512514	.513598
10/12/2020	40	A	9	.523529	.521533	.507900	.507632	.517669	.517100	.507597	.516894
10/12/2020	41	A	9	.523529	.520452	.514699	.514738	.519359	.519186	.514732	.519097
10/12/2020	42	A	9	.523529	.518271	.516340	.516407	.518264	.518232	.516340	.518147

10/12/2020	43	A	9	.523529	.517873	.509417	.515072	.515371	.517389	.523564	.523589
<b>Actual and Predicted Chl-a Concentrations by Model (continued)</b>											
11/11/2020	104	C	9	.515444	.513642	.511226	.511140	.512735	.512617	.511165	.512607
11/11/2020	104	D	9	.506641	.504497	.504727	.504219	.503157	.502944	.504030	.502830
11/11/2020	105	B	9	.499065	.507178	.509379	.509208	.506990	.506986	.509224	.507040
11/11/2020	106	B	9	.499065	.505510	.512610	.512589	.506890	.507114	.512624	.507244
11/11/2020	107	B	9	.499065	.513030	.518468	.518553	.514958	.515179	.518380	.515117
11/11/2020	108	B	9	.499065	.516965	.519819	.519895	.518540	.518675	.519628	.518501
11/11/2020	108	E	9	.510516	.504612	.513541	.513544	.506535	.506831	.513556	.506968
11/11/2020	109	A	9	.497207	.507641	.515152	.515194	.509505	.509772	.515163	.509853
11/11/2020	109	F	9	.510516	.504514	.512798	.512783	.506181	.506447	.512814	.506591
11/11/2020	110	A	9	.497207	.510298	.514225	.514247	.511238	.511378	.514246	.511431
11/11/2020	110	F	9	.510516	.500100	.510042	.509912	.501700	.501970	.509947	.502147
11/11/2020	111	B	9	.499065	.519662	.514785	.514807	.518772	.518622	.514771	.518523
11/11/2020	112	B	9	.499065	.510126	.508250	.508000	.508875	.508703	.507969	.508668
11/11/2020	113	B	9	.499065	.507435	.503949	.503350	.505166	.504792	.503076	.504563
11/11/2020	114	B	9	.499065	.504469	.499435	.498349	.501162	.500532	.497646	.499973
11/11/2020	120	A	9	.497207	.504546	.504628	.504106	.503159	.502935	.503903	.502809
11/11/2020	120	F	9	.510516	.504800	.502626	.501913	.502611	.502231	.501556	.501963
11/11/2020	121	A	9	.497207	.501784	.505710	.505286	.501402	.501347	.505159	.501328
11/11/2020	121	F	9	.510516	.506014	.506327	.505946	.504941	.504785	.505844	.504732
11/11/2020	122	A	9	.497207	.501710	.505914	.505502	.501420	.501379	.505381	.501369
11/11/2020	122	F	9	.510516	.504716	.505798	.505373	.503729	.503579	.505241	.503516
11/11/2020	123	A	9	.497207	.505366	.500593	.499652	.502296	.501735	.499088	.501280
10/12/2020	16	A	20	.523529	.516658	.525513	.525331	.520367	.520313	.525515	.520371
10/12/2020	16	B	20	.523529	.527017	.521468	.521415	.526786	.526814	.521488	.526802
10/12/2020	16	F	20	.518447	.523802	.520885	.520843	.524112	.524134	.520905	.524130
10/12/2020	17	A	20	.523529	.519049	.525203	.525037	.522080	.522040	.525209	.522086
10/12/2020	17	B	20	.523529	.520171	.519192	.519175	.520710	.520728	.519211	.520728
10/12/2020	17	F	20	.518447	.519169	.519501	.519479	.520059	.520072	.519520	.520077
10/12/2020	18	B	20	.523529	.511646	.517668	.517660	.513631	.513623	.517683	.513647

10/12/2020	18	F	20	.518447	.519020	.516148	.516123	.518704	.518715	.516152	.518708
<b>Actual and Predicted Chl-a Concentrations by Model (continued)</b>											
10/12/2020	19	B	20	.523529	.516278	.516529	.516514	.516749	.516754	.516538	.516757
10/12/2020	19	E	20	.522505	.528380	.517840	.517828	.526483	.526531	.517855	.526494
10/12/2020	20	E	20	.522505	.525264	.512931	.512859	.522284	.522298	.512910	.522262
10/12/2020	27	B	20	.523529	.525292	.513284	.513219	.522437	.522453	.513266	.522418
10/12/2020	28	B	20	.523529	.521077	.519122	.519104	.521377	.521398	.519141	.521394
10/12/2020	29	A	20	.523529	.520464	.518121	.518114	.520538	.520561	.518139	.520554
10/12/2020	29	B	20	.523529	.522607	.521083	.521039	.523273	.523290	.521103	.523291
10/12/2020	30	A	20	.523529	.515949	.519019	.519008	.517420	.517426	.519039	.517439
10/12/2020	31	A	20	.523529	.514079	.521113	.521070	.516767	.516754	.521134	.516787
10/12/2020	32	A	20	.523529	.514141	.521415	.521365	.516926	.516911	.521435	.516945
10/12/2020	33	A	20	.523529	.510507	.517140	.517131	.512566	.512553	.517153	.512579
10/12/2020	34	A	20	.523529	.513941	.511456	.511318	.513085	.513035	.511412	.513044
10/12/2020	34	B	20	.523529	.527528	.520377	.520355	.526772	.526814	.520400	.526791
10/12/2020	35	B	20	.523529	.517342	.517219	.517211	.517818	.517829	.517233	.517830
10/12/2020	36	B	20	.523529	.514760	.512871	.512800	.514235	.514213	.512850	.514215
10/12/2020	40	A	20	.523529	.521054	.507754	.507433	.517150	.517056	.507646	.517049
10/12/2020	41	A	20	.523529	.520095	.514961	.514933	.519086	.519098	.514960	.519083
10/12/2020	42	A	20	.523529	.517710	.515884	.515870	.517605	.517615	.515891	.517610
10/12/2020	43	A	20	.523529	.516976	.515222	.515200	.516799	.516803	.515224	.516800
11/11/2020	104	C	20	.515444	.513176	.511371	.511239	.512469	.512418	.511328	.512429
11/11/2020	104	D	20	.506641	.504348	.505128	.504619	.503410	.503189	.504960	.503258
11/11/2020	105	B	20	.499065	.506537	.509994	.509807	.506885	.506791	.509930	.506828
11/11/2020	106	B	20	.499065	.506718	.512984	.512908	.508131	.508080	.512962	.508113
11/11/2020	107	B	20	.499065	.513520	.518201	.518193	.515261	.515259	.518219	.515278
11/11/2020	108	B	20	.499065	.517300	.520446	.520415	.518981	.518984	.520467	.519001
11/11/2020	108	E	20	.510516	.504667	.512977	.512904	.506560	.506503	.512956	.506543
11/11/2020	108	F	20	.510516	.513764	.514720	.514687	.514158	.514147	.514717	.514155
11/11/2020	109	A	20	.497207	.507637	.515665	.515642	.509826	.509798	.515668	.509831
11/11/2020	109	F	20	.510516	.505136	.513181	.513114	.506995	.506941	.513162	.506980

11/11/2020	110	A	20	.497207	.510198	.513877	.513826	.511121	.511091	.513865	.511112
<b>Actual and Predicted Chl-a Concentrations by Model (continued)</b>											
11/11/2020	110	F	20	.510516	.500803	.510711	.510559	.502768	.502668	.510660	.502724
11/11/2020	111	B	20	.499065	.517970	.514811	.514766	.517406	.517406	.514805	.517400
11/11/2020	112	B	20	.499065	.508737	.508529	.508259	.508024	.507907	.508437	.507941
11/11/2020	113	B	20	.499065	.504992	.503847	.503220	.503428	.503165	.503642	.503243
11/11/2020	114	B	20	.499065	.504430	.500018	.498990	.501581	.501166	.499692	.501285
11/11/2020	120	A	20	.497207	.504143	.504975	.504456	.503197	.502971	.504803	.503042
11/11/2020	120	F	20	.510516	.503317	.502810	.502087	.501764	.501459	.502576	.501552
11/11/2020	121	A	20	.497207	.501567	.506349	.505938	.501737	.501543	.506211	.501614
11/11/2020	121	F	20	.510516	.504585	.506002	.505555	.503915	.503717	.505854	.503781
11/11/2020	122	A	20	.497207	.502180	.500486	.506305	.500035	.502150	.501957	.501371
11/11/2020	122	F	20	.510516	.505388	.502637	.506027	.503283	.504509	.503480	.504049
11/11/2020	123	A	20	.497207	.504946	.500549	.499584	.502172	.501783	.500242	.501893
11/11/2020	124	A	20	.497207	.500630	.497481	.496129	.497737	.497189	.497060	.497355
10/12/2020	16	A	50	.523529	.515228	.525622	.525190	.520530	.520322	.524776	.520824
10/12/2020	16	B	50	.523529	.524918	.522041	.521845	.525301	.525196	.521654	.525461
10/12/2020	16	F	50	.518447	.523035	.521345	.521191	.523715	.523631	.521041	.523840
10/12/2020	17	A	50	.523529	.518336	.524943	.524562	.522282	.522096	.524197	.522549
10/12/2020	17	B	50	.523529	.518702	.519775	.519704	.520082	.520042	.519632	.520137
10/12/2020	17	F	50	.518447	.517736	.519395	.519341	.519257	.519226	.519284	.519298
10/12/2020	18	B	50	.523529	.512498	.517731	.517746	.514975	.514982	.517755	.514954
10/12/2020	18	F	50	.518447	.517099	.515971	.516037	.517213	.517239	.516094	.517172
10/12/2020	19	B	50	.523529	.514725	.516290	.516350	.515779	.515805	.516402	.515735
10/12/2020	19	E	50	.522505	.525223	.517458	.517472	.523336	.523330	.517481	.523354
10/12/2020	20	E	50	.522505	.523121	.513109	.513237	.519876	.519926	.513355	.519814
10/12/2020	26	B	50	.523529	.520150	.515251	.515346	.518908	.518945	.515432	.518857
10/12/2020	27	B	50	.523529	.523581	.514360	.514472	.520775	.520817	.514573	.520724
10/12/2020	28	A	50	.523529	.524354	.516067	.516149	.522098	.522125	.516223	.522067
10/12/2020	28	B	50	.523529	.519314	.519421	.519370	.520323	.520291	.519316	.520366
10/12/2020	29	A	50	.523529	.519192	.517125	.517150	.519155	.519159	.517168	.519148

10/12/2020	29	B	50	.523529	.520587	.521702	.521531	.522251	.522162	.521363	.522381
<b>Actual and Predicted Chl-a Concentrations by Model (continued)</b>											
10/12/2020	30	A	50	.523529	.514237	.519341	.519287	.516897	.516869	.519230	.516928
10/12/2020	31	A	50	.523529	.513421	.521609	.521443	.517426	.517346	.521281	.517529
10/12/2020	32	A	50	.523529	.513658	.521887	.521703	.517715	.517626	.521523	.517833
10/12/2020	33	A	50	.523529	.510837	.516252	.516314	.513168	.513198	.516367	.513111
10/12/2020	34	A	50	.523529	.513611	.511624	.511747	.512829	.512886	.511862	.512745
10/12/2020	34	B	50	.523529	.523268	.520041	.519967	.523254	.523208	.519892	.523324
10/12/2020	35	A	50	.523529	.518319	.509560	.509694	.514994	.515052	.509822	.514920
10/12/2020	35	B	50	.523529	.517106	.516561	.516618	.517497	.517519	.516667	.517461
10/12/2020	36	B	50	.523529	.513919	.511954	.512092	.513191	.513255	.512221	.513097
10/12/2020	37	B	50	.523529	.515148	.511179	.511326	.513644	.513711	.511465	.513548
10/12/2020	40	A	50	.523529	.519678	.507713	.507789	.515026	.515056	.507864	.515002
10/12/2020	41	A	50	.523529	.517849	.514305	.514416	.516925	.516972	.514517	.516857
10/12/2020	42	A	50	.523529	.516646	.515903	.515978	.516878	.516909	.516043	.516830
10/12/2020	43	A	50	.523529	.516226	.515397	.515485	.516358	.516396	.515564	.516300
11/11/2020	104	B	50	.499065	.511844	.508350	.508467	.510101	.510157	.508580	.510022
11/11/2020	104	C	50	.515444	.511800	.510474	.510606	.511077	.511140	.510730	.510983
11/11/2020	104	D	50	.506641	.503619	.504053	.504030	.502581	.502579	.504017	.502587
11/11/2020	105	B	50	.499065	.506675	.509614	.509750	.507250	.507321	.509878	.507141
11/11/2020	106	B	50	.499065	.507060	.512902	.513032	.509063	.509130	.513153	.508952
11/11/2020	107	B	50	.499065	.512605	.518085	.518090	.515214	.515216	.518089	.515200
11/11/2020	107	E	50	.510516	.504807	.510561	.510708	.506452	.506529	.510847	.506326
11/11/2020	108	A	50	.497207	.522782	.515733	.515808	.520892	.520917	.515874	.520862
11/11/2020	108	B	50	.499065	.516607	.520618	.520505	.519083	.519025	.520393	.519160
11/11/2020	108	E	50	.510516	.505602	.512597	.512732	.507945	.508016	.512857	.507827
11/11/2020	108	F	50	.510516	.512402	.514315	.514427	.513295	.513348	.514530	.513211
11/11/2020	109	A	50	.497207	.507465	.515225	.515313	.510432	.510478	.515392	.510348
11/11/2020	109	E	50	.510516	.517674	.515849	.515917	.517538	.517565	.515977	.517498
11/11/2020	109	F	50	.510516	.505611	.512891	.513020	.508091	.508159	.513138	.507977
11/11/2020	110	A	50	.497207	.508916	.512914	.513045	.510307	.510372	.513166	.510201

11/11/2020	110	E	50	.510516	.509570	.511534	.511668	.510091	.510157	.511793	.509987
<b>Actual and Predicted Chl-a Concentrations by Model (continued)</b>											
11/11/2020	110	F	50	.510516	.501920	.509878	.510017	.504203	.504279	.510148	.504076
11/11/2020	111	A	50	.497207	.509483	.509166	.509300	.508912	.508978	.509428	.508812
11/11/2020	111	B	50	.499065	.517378	.514703	.514796	.516798	.516837	.514880	.516741
11/11/2020	111	E	50	.510516	.504256	.504893	.504903	.503403	.503416	.504919	.503387
11/11/2020	111	F	50	.510516	.504170	.507245	.507341	.504458	.504512	.507436	.504374
11/11/2020	112	B	50	.499065	.508845	.508062	.508170	.507964	.508019	.508273	.507885
11/11/2020	113	B	50	.499065	.505089	.502833	.502750	.502984	.502953	.502683	.503040
11/11/2020	114	B	50	.499065	.504115	.498881	.498543	.500465	.500314	.498242	.500711
11/11/2020	117	B	50	.499065	.495933	.498161	.497802	.494665	.494512	.497482	.494903
11/11/2020	118	B	50	.499065	.505330	.503171	.503114	.503305	.503286	.503071	.503342
11/11/2020	119	B	50	.499065	.512966	.505365	.505385	.509437	.509447	.505410	.509438
11/11/2020	120	A	50	.497207	.503616	.503987	.503969	.502548	.502548	.503959	.502552
11/11/2020	120	F	50	.510516	.503441	.502326	.502209	.501644	.501599	.502111	.501722
11/11/2020	121	A	50	.497207	.502214	.505656	.505702	.502402	.502434	.505751	.502351
11/11/2020	121	F	50	.510516	.504696	.505361	.505393	.503918	.503941	.505429	.503886
11/11/2020	122	A	50	.497207	.503023	.506089	.506149	.503146	.503184	.506210	.503088
11/11/2020	122	F	50	.510516	.505485	.505753	.505799	.504629	.504659	.505848	.504588
11/11/2020	123	A	50	.497207	.503720	.498855	.498515	.500189	.500038	.498211	.500436
11/11/2020	124	A	50	.497207	.501604	.497006	.496514	.497902	.497681	.496071	.498256